

# Evaluating Adversarial Robustness of Convolution-based Human Motion Prediction

Chengxu Duan, Zhicheng Zhang, Xiaoli Liu, Yonghao Dang and Jianqin Yin \*

*the School of Artificial Intelligence, Beijing University of Posts and Telecommunications, Beijing, China*

## Abstract

Human motion prediction has achieved a brilliant performance with the help of CNNs, which facilitates human-machine cooperation. However, currently, there is no work evaluating the potential risk in human motion prediction when facing adversarial attacks, which may cause danger in real applications. The adversarial attack will face two problems against human motion prediction: 1. For naturalness, pose data is highly related to the physical dynamics of human skeletons where  $L_p$  norm constraints cannot constrain the adversarial example well; 2. Unlike the pixel value in images, pose data is diverse at scale because of the different acquisition equipment and the data processing, which makes it hard to set fixed parameters to perform attacks. To solve the problems above, we propose a new adversarial attack method that perturbs the input human motion sequence by maximizing the prediction error with physical constraints. Specifically, we introduce a novel adaptable scheme that facilitates the attack to suit the scale of the target pose and two physical constraints to enhance the imperceptibility of the adversarial example. The evaluating experiments on three datasets show that the prediction errors of all target models are enlarged significantly. Specifically, the results when facing the weakest attack in the experiment setting increase by 22% at least, 295% at most, which means current convolution-based human motion prediction models can be easily disturbed under the proposed attack. The quantitative analysis shows that prior knowledge and semantic information modeling can be the key to the adversarial robustness of human motion predictors. The qualitative results indicate that the adversarial sample is hard to be noticed when compared frame by frame but is relatively easy to be detected when the sample is animated. We also explore the contribution of different frames in the input sequence to the prediction results, which shows that the observed frame can be the weak point in the input. The code will be available in the future.

## 1 Introduction

Driven by Convolutional Neural Networks(CNNs), recent works in Human Motion Prediction(HMP) have achieved excellent performance [1–3], which facilitates many applications such as intelligent security, autonomous driving, human-machine interaction, and so on. Specifically, motion prediction forecasts the future motion of the target person according to the observed poses. Human motion prediction is a fundamental ability that helps humans prepare in advance during interactions like catching. Similarly, precise motion prediction helps robot agents learn the future human posture and ensures the safety and smoothness of human-machine cooperation.

---

\*Corresponding author: jqyin@bupt.edu.cn

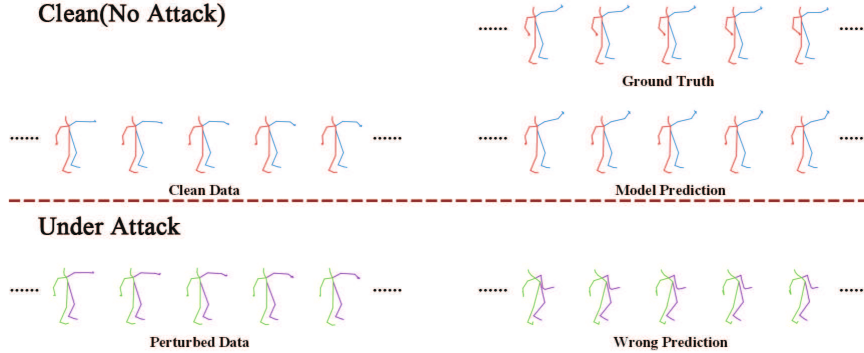


Figure 1: An example of the proposed attack against human motion prediction. The poses above the red line are the clean input and output of human motion prediction; the poses below the red line are the perturbed input and output of the prediction, which is obvious that the difference between the clean data and the perturbed data is imperceptible while the disturbance in prediction is significant.

However, recent research has proved that CNNs are vulnerable to adversarial attacks [4]. Adversarial attacks can be achieved by generating adversarial examples, a combination of clean samples, and quasi-perceptible noises designed deliberately, eventually misleading the prediction of deep learning models. Since discovering the existence of adversarial examples, many works have stimulated the research of adversarial attacks [4–14], which alarms algorithm designers about the necessity of adversarial robustness in real scenarios. Currently, the scope of adversarial attacks has extended to other tasks [15–21].

Nevertheless, to the best of our knowledge, there is no related work that considers evaluating the adversarial robustness of human motion prediction tasks. Human motion prediction is essential for robot agents to interact with humans correctly. A wrong prediction of the future human pose can hinder the robot agent from completing tasks or even mislead the agent to directly hit a human, which may cause danger when facing a high-power robot. For example, in industrial applications, robot arms may avoid workers’ bodies and finish their job simultaneously, which realized that humans and robots work in the same space. However, robot arms under attack may predict workers’ motion in the wrong place, swing their arms vigorously, and cause injuries to workers. To deal with the problem above in analyzing the potential threat from adversarial attacks, we propose a new white-box adversarial attack method against convolution-based human motion prediction models to evaluate their adversarial robustness. To satisfy the requirement of an adversarial attack for harmfulness and naturalness, the proposed attack method combines a clean human motion sequence and a set of minor adversarial vectors pointing to the susceptible direction of each joint to maximize the prediction error meanwhile considering the naturalness of human skeletons.

Compared with adversarial attacks on image classification, attacking human motion prediction is highly challenging in two aspects. First, existing adversarial attack works can be used to disturb the motion prediction models, but the  $L_p$  norm constraint they deploy may cause physical unnaturalness in the human skeleton [18–21], which doesn’t meet the requirement of adversarial attacks for imperceptibility. To tackle this problem, we design two constraints for our attack method: temporal loss and bone length loss. Temporal loss aims to limit the change of joints’ speed and its derivatives between the clean poses and the adversarial poses, while bone length loss aims to avoid obvious deformation of each bone in the skeleton. Second, the coordinates of the human skeleton taken by different equipment are not uniform in scale. Thus, we design a practical scheme to help the proposed attack suit the scale of the target skeleton

automatically, making it easy to attack different datasets.

In the proposed attack, the method first calculates the scale of the input sequence in the proposed scheme. Then the method optimizes the adversarial perturbation by maximizing the prediction error to produce the attack effectiveness and minimizing the proposed loss to ensure the naturalness of the adversarial example. Finally, while the optimization process makes the adversarial perturbation more and more harmful, a hard constraint is needed to ensure the adversarial example sneaky during the iterations. After each iteration, the method clips the perturbation by the  $L_\infty$  norm constraint and gets the optimal adversarial perturbation when the maximum number of iterations is reached.

We evaluate the adversarial robustness of four different models [1, 2, 22, 23] on three datasets [24–26] by the proposed attack method. The attack effectiveness is shown in Figure 1. The results show that the proposed attack is successful across datasets and models. Even the smallest perturbation can significantly enlarge the prediction error of all models by 22% at least and 295% at most, indicating the vulnerability of current human motion prediction algorithms. Comparing the results of each target model, we discover that prior knowledge and semantic information modeling can be the key to adversarial robustness. According to the qualitative results, the adversarial sample is almost the same as the clean sample to human eyes, but it is relatively more noticeable when the motion information is animated. In general, the proposed attack successfully evaluates the adversarial robustness of the target models, which alarms that designers should be attached weight to the adversarial robustness of human motion prediction.

Our main contributions are summarized as follows:

1. To the best of our knowledge, we propose the *first* adversarial attack method to evaluate the adversarial robustness of human motion prediction. Inspired by [19], we constrain the perturbation optimization from both temporal feature and spatial feature, which enhances the imperceptibility of the adversarial example;
2. We propose a novel adaptable scheme for the proposed attack method to suit the scale of the input motion sequence automatically, which solves the inconsistency of the data scales between different datasets and maximizes the attack effectiveness meanwhile ensuring the naturalness of the attack;
3. We thoroughly evaluate the adversarial robustness of various prediction models under the proposed attack on different human motion datasets. The evaluation results show the vulnerability of the current models and reveal the keys to the adversarial robustness of human motion prediction.

## 2 Related Works

### 2.1 Convolution-based Human Motion Prediction

With the brilliant ability to capture spatial and temporal features of human poses, CNNs are widely used in human motion prediction. The conventional CNN structure treats human motion sequences as a series of 2D data and extracts their feature effectively [22, 27–29]. Butepage et al. [27] utilized CNN to learn a generic representation that can be generalized to unseen future motions. Li et al. [28] supported RNN network by CNN to model spatial dependencies in human motion sequences. Li et al. [29] designed a convolutional hierarchical autoencoder framework to exploit the human body constraints efficiently. Liu et al. [22] proposed a spatiotemporal feature learning CNN network, TrajectoryCNN, to capture the motion dynamics of the previous human motion sequence in the trajectory space and predict future human motion sequences in a non-recursive manner. However, conventional CNNs can capture the local features of human motion well but may neglect the global features.

As the skeleton-based human pose data are highly structured and can be presented by priori knowledge graphs, GCNs are popular in recent works, which can consider the local and global information

of the human motion data at the same time. Mao et al. [1] first encoded the human skeleton as a graph structure and then captured spatial dependencies by GCN.

With the help of the graph, the GCN-based model can explore the inner relations of the human body [26, 30–32]. Li et al. [30] designed a novel GCN containing a multi-scale graph to represent the human skeleton and used a graph-based GRU to predict future poses. Dang et al. [26] proposed a novel multi-scale residual graph convolution network whose ascending and descending blocks realized capturing fine-to-coarse and coarse-to-fine features.

Furthermore, human motion dynamics are also highly related to the temporal relationship, which developed into spatio-temporal relationships that need to be analyzed in GCN [3, 33–37]. Lebailly et al. [33] embedded human motion sequence into trajectories, then obtained residual motion prediction using GCN. Zhong et al. [36] adopted the gating network to enhance the generalization of GCN on human motion prediction. Sofianos et al. [37] proposed a method that factorizes the graph adjacency matrix and extracts the interactions of joint-to-joint, time-to-time, and joint-to-time by GCNs.

What’s more, GCN can fuse with other networks to achieve improvement [2, 38–40]. Chao et al. [38] combined GCN structure and adversarial training to refine predicted human motion. Li et al. [39] designed a multiscale spatiotemporal graph computing unit with GCN as the core part of the encoder and a graph-based GRU as the decoder. Wei et al. [2] applied attention mechanism to GCN structure, which unifies the short-term and long-term prediction and enhances the ability of the network to make use of motion repetitiveness. However, the relation described by the adjacent matrix may be rigid, which makes the network hard to understand the dynamic relationships between the joints in the human skeleton.

Although the above works achieve excellent performance, they don’t consider the adversarial robustness of motion prediction networks, which is not safe to deploy these models into real scenarios. In this paper, we focus on the adversarial robustness of current human motion prediction algorithms.

## 2.2 Adversarial Attack

Since Szegedy et al. [4] finds that a series of quasi-perceptible perturbations can be designed to mislead deep learning network malfunctioning, plenty of works have proved the vulnerability of DNN in image classification [4–13].

Among previous works of adversarial attack, optimization-based attack methods [4, 6, 8, 11, 12], which generate noises according to the gradient of the loss function or the score function corresponding to the network, can be easily generalized to perturb most of the DNNs. For instance, Fast Gradient Sign Method (FGSM) [13] directs the adversarial perturbation by the grad of input images and the sign function and constrains its magnitude by just one parameter, which realizes a one-step attack. Projected Gradient Descend (PGD) [6] generates perturbations by accumulating grads from each iteration perturbed images’ backward propagation, which is proved to be the strongest attack utilizing the local first-order information about the network [6]. Meanwhile, optimization-based methods spread to other tasks like semantic segmentation [15], autonomous driving [16], and pose estimation [14, 17] for evaluating the adversarial robustness of corresponding models.

The adversarial attack has involved human pose space in action recognition [18–21] and shown that perturbations against skeleton-based data need to be restricted physically. Liu et al. [18] proposed the first adversarial attack on deep skeleton action recognition, which perturbs the input data from a spatio-temporal perspective. Wang et al. [19] designed a new perceptual loss to constrain the perturbation, analyzed the adversarial robustness of action recognition models, and showed the difference between attacking images and skeletons: Unlike image data, human skeleton data are highly related to physical constraints and have much fewer Degrees of Freedom (DoFs) than image data, making human skeleton data low redundant and perceptual sensitive [19, 20]. Diao et al. [20] proposed the first black-box attack

on action prediction, which misleads the data to leave the correct classification distribution in the shortest distance and applies inverse kinematics to make the skeleton natural visually.

However, to the best of our knowledge, no existing work studied the adversarial robustness of human motion prediction, which may cause fatal mistakes in human-machine interaction. For this reason, we propose an adversarial attack method against motion prediction to evaluate its potential problem.

## 3 Problem Formulation

### 3.1 Human Motion Prediction

In this work, we focus on human motion prediction, which is executed to forecast a future human motion sequence according to the corresponding past human motion sequence. First, we denote  $s_i$  as a true pose composed of  $J$  joint points at time  $i$ , and each joint point has  $D$  dimensions. Then we can denote  $X = \{s_1, s_2, \dots, s_{T_h}\}, X \in R^{T_h \times J \times D}$  as an observed motion sequence of length  $T_h$  and  $Y = \{s_{T_h+1}, s_{T_h+2}, \dots, s_{T_h+T_f}\}, Y \in R^{T_f \times J \times D}$  as the future ground truth motion sequence of length  $T_f$ . This work focuses on Cartesian coordinates; therefore,  $D$  equals 3. The prediction algorithm inputs the history human motion sequence  $X$  and generates the predicted human motion sequence  $P = \{\hat{s}_{T_h+1}, \hat{s}_{T_h+2}, \dots, \hat{s}_{T_h+T_f}\}, P \in R^{T_f \times J \times D}$  where  $\hat{s}_i$  is the predicted pose at time  $i$ . During training, the sequence  $P$  is optimized to approximate the distribution of the future ground-truth motion sequence  $Y$ . Therefore, the prediction algorithms can output generally precise future poses.

### 3.2 Attack Model

In this paper, we focus on the scenario that human joints' locations can be directly acquired by motion capture (e.t. MoCap) techniques. In this setting, human joints are recognized as rotation angles or 3D coordinates, which can be connected as a graph known as a skeleton. Based on human motion sequences, prediction algorithms model the spatiotemporal feature of the target and construct the motion dynamics of the target movement. On the contrary, the adversarial attack aims to disrupt the normal operation of the model without being perceived by human users. Thus, the adversary needs to perturb the history human motion sequence so that the prediction algorithm will mislead the motion in an utterly wrong direction, which may disturb the user's prediction of the future human motion sequence. Such mistakes can cause users or robots to take wrong actions, which may lead to fatal damage.

Our goal is to analyze the adversarial robustness of current human motion prediction algorithms by an adversarial attack that can find worst-case perturbation against the algorithm while keeping the adversarial examples natural. Therefore, the problem can be described as follows: given a history human motion sequence  $X$  with its future ground truth  $Y$ , the proposed attack aims to find  $X'$  that is visually similar to  $X$  and can fool the white-boxed predictor such that the error between the predicted sequence  $P$  and  $Y$  is maximized.

Based on optimization-based methods, the proposed attack formulates the problem as a constrained optimization problem, which can be solved by gradient descent. Because human pose data are low redundant and perceptual sensitive [19, 20], the adversarial perturbation for human motion sequences needs to be bounded by the  $L_p$  norm and constrained by physical laws. In the proposed attack, the physical constraints are formulated as two loss functions to constrain the spatial feature of the pose and the temporal feature of the pose, respectively. Therefore, the solution of the proposed perturbation can be defined as:

$$\begin{aligned} & \max_{X'} L_{pred}(f(X'), Y) - \lambda \cdot L_{phy}(X, X') \\ & s.t. \|X' - X\|_p \in [0, \varepsilon] \end{aligned} \quad (1)$$

where  $L_{pred}(\cdot)$  denotes the prediction error function of human motion prediction,  $L_{phy}(\cdot)$  denotes the integrated physical constraint function,  $f(\cdot)$  denotes the target human motion prediction model,  $X'$  denotes the adversarial example,  $\lambda$  is a trade-off parameter between attack effectiveness and naturalness, and  $\varepsilon$  is the boundary of the adversarial perturbation.

## 4 Methodology

### 4.1 Optimization for Attack

The basic objective of our attack is to deviate the prediction poses away from the true future poses; the further, the better. The proposed attack method generates adversarial samples by adding a minor perturbation to the original history trajectories. From the perspective of human posture, the perturbation, which can be regarded as a series of vectors, changes the 3D coordinates of each joint in human skeleton data and further sabotages the spatiotemporal features of the history motion sequence, which cause an utterly wrong prediction. In a realistic scenario, because the risk will accumulate as time passes, and the attack will work better when it has more parameters to perturb, the proposed attack will target the whole history sequence as the input data.

According to Equation (1), the attack effectiveness is based on maximizing the prediction error of the human motion prediction model, which indicates  $L_{pred}$ . Specifically, the basic optimization goal to generate attack effectiveness is the negation of the average prediction error of each joint in all considered time frames. For a single motion sequence, the  $L_{pred}$  is formulated as:

$$L_{pred}(P, Y) = \frac{1}{T_f \cdot J} \sum_{i=1}^{T_f} \sum_{j=1}^J \|\hat{s}_{T_h+i,j} - s_{T_h+i,j}\|_2 \quad (2)$$

where  $\hat{s}_{T_h+i,j}$  and  $s_{T_h+i,j}$  denote the  $j$  joint coordinate in frame  $i$  respectively from the prediction motion sequence  $P$  and the true future motion sequence  $Y$ , which are defined in 3.1.  $T_h$  and  $T_f$  are the length of the history motion sequence and the future motion sequence.  $J$  is the number of joints in the human skeleton.

### 4.2 Constraints for Perceptual Naturalness

As mentioned in 3.2, human motion sequence data must be physically natural. As a result, we design a scheme and two constraints to enforce the adversarial sequence obeying the physical law.

**Adaptable Scheme** According to our observation, the scale of the skeleton data varies across different datasets, so it is not a good idea to use constant parameters to manipulate the vectors in adversarial perturbation. To solve this problem, we propose an adjustable scale function  $S_c$  for each batch:

$$\begin{aligned} f_{span}^x(X) &= \min(\max(X^x) - \min(X^x)) \\ S_c(X) &= \min(f_{span}^x(X), f_{span}^y(X), f_{span}^z(X)) \end{aligned} \quad (3)$$

where  $X$  denotes the history human motion sequence;  $x$ ,  $y$ , and  $z$  denote the dimension that the function needs to measure, and  $X^x$  denotes all the  $x$ -coordinate in the history motion sequence, similar to  $X^y$  and  $X^z$ ;  $\min(\cdot)$  and  $\max(\cdot)$  denote picking the minimum and maximum of the sequence, respectively.

In the proposed scheme, the scale function first finds a basic unit, and then the proposed attack utilizes this unit to perform operations like update and clip. In this scheme, we assume there is a bounding box that can just fit the target pose. Then the scale function will calculate the minimum side lengths on each axis and choose the shortest one as the basic unit to perform the adversarial attack. As a result, the proposed scheme can help the attack adapt to each input sequence and facilitate users setting a set of unified parameters for the attack.

**Physical Constraints** To constrain the physical characteristic of the adversarial sample, the optimization needs to consider the temporal features of each joint and spatial features between specified joints. The spatiotemporal feature needs to be constrained by  $L_{phy}$  in Equation(1) composed of a temporal constraint  $L_{temp}$  and a spatial constraint  $L_{BL}$ .

For the temporal feature, inspired by [19], the speed of each joint and its derivatives shouldn't change significantly between each frame. According to this hypothesis, the attack minimizes the following loss function to constrain the perturbation:

$$L_{temp}(X, X') = \frac{1}{N} \sum_{n=1}^N \|X^{(n)} - X'^{(n)}\|_2 \quad (4)$$

where  $X$  denotes the history motion sequence while  $X'$  denotes the adversarial motion sequence.  $X^{(n)}$  denotes the  $n$ -th derivative of the sequence  $X$ , which is similar to  $X(n)$ .  $N$  denotes the number of differential orders. In this work, we only consider an intuitive way to constrain each joint's velocity and acceleration, so we set  $N$  as 2. During the optimization, the adversarial perturbation needs to minimize  $L_{temp}$  so that the joints will not be moved too randomly and look like the target is shaking.

As for the spatial feature, bone length is a sensitive attribute. Without constraining the bone length, the limbs in the adversarial sequence will be elastic, which can be detected by human eyes easily. Therefore, the proposed attack calculates the length of each bone in every pose and minimizes the error between the adversarial and the clean. We apply the bone length loss function from [19] to constrain the motion:

$$L_{BL}(X, X') = \|BL(X) - BL(X')\|_2 \quad (5)$$

where  $BL(\cdot)$  denotes the function that calculates the length of all bones in the sequence based on its corresponding skeleton structure. By minimizing  $L_{BL}$ , the influence of adversarial perturbations on poses' bones can be largely decreased, enhancing the attack's imperceptibility. In conclusion, the goal of our attack method is to maximize the following loss:

$$\begin{aligned} L &= L_{pred} - \lambda \cdot L_{phy} \\ L_{phy} &= L_{temp} + L_{BL} \end{aligned} \quad (6)$$

where  $\lambda$  denotes the trade-off parameter between the attack effectiveness and perceptual naturalness. After the scale  $S_c(X)$  and the integrated loss  $L$  are calculated, we can apply the proposed scheme to update the adversarial motion sequence by the following equation:

$$\begin{aligned} X' &= Clip_{X, \varepsilon \cdot S_c(X)} \{X' + \varepsilon_{step} \cdot S_c(X) \cdot sign(\nabla L_{X'})\} \\ \|X' - X\|_\infty &\leq \varepsilon \cdot S_c(X) \end{aligned} \quad (7)$$



where  $X'$  denotes the perturbed history sequence;  $\varepsilon$  denotes the parameter that bounds the perturbation.  $Clip_{X,\varepsilon,S_c(X)}$  function clips deviations in each axis so that the absolute distances of the adversarial example in each axis will not exceed  $\varepsilon \cdot S_c(X)$  away from the clean example  $X$ .  $\varepsilon_{step}$  denotes the step-size parameter.  $\nabla L_{X'}$  computes the gradient of the integrated loss function  $L$  around the current adversarial example  $X'$ , and  $sign(\cdot)$  is the sign function. With the help of the scale function, we enhance perturbation imperceptibility in a traditional  $L_\infty$ -norm way.

### 4.3 Generation of Perturbations

---

**Algorithm 1** Overview of the proposed attack scheme

---

**Input:** history sequence  $X$ , future sequence  $Y$ , target model  $f(\cdot)$ , boundary  $\varepsilon$ , iteration number  $N$ , step size  $\varepsilon_{step}$

**Output:** perturbed sequence  $X'$

- 1: **Initialization:** Calculate the scale of  $X$  by Equation (3) Initialize perturbation  $S_{pert}$  randomly under  $\varepsilon \cdot S_c(X)$
  - 2: **for**  $doi = 1, 2, \dots, N$
  - 3:      $X' = X + S_{pert}$
  - 4:     Turn  $X'$  into the form the model needs
  - 5:      $P = f(X')$
  - 6:     Calculate  $L_{pred}, L_{temp}, L_{BL}$  by Equation(2)(4)(5)
  - 7:      $L = L_{pred} - \lambda \cdot (L_{temp} + L_{BL})$
  - 8:      $X' = Clip_{X,\varepsilon,S_c(X)} \{X' + \varepsilon_{step} \cdot S_c(X) \cdot sign(\nabla L_{X'})\}$
  - 9: **end for**
- 

Our optimization method is based on Projected Gradient Descent (PGD) [6]. The process is summarized in Algorithm 1.

Following the proposed scheme, The perturbation is initialized randomly, and then the input scale is calculated to ensure the size of the poses. We first add the current perturbation to each iteration’s clean history human motion sequence. Next, the model predicts a human motion sequence based on the perturbed input sequence. Then the algorithm calculates  $L$  based on Equation (7) and updates the perturbation by gradient descent under the control of the scale function. Finally, the algorithm generates the adversarial perturbation, which can mislead motion prediction to a series of wrong poses.

## 5 Experiment

### 5.1 Experimental Settings

In this section, we will introduce the datasets(5.1.1), the target baselines(5.1.2), the evaluation metrics(5.1.3), and the implementing details(5.1.4) set in the evaluation experiment.

#### 5.1.1 Datasets

In the experiment, we choose Human 3.6M [24](H3.6M), CMU-Mocap(CMU)<sup>1</sup>, and 3D Pose in the Wild dataset [25](3DPW) as the evaluation dataset. Human3.6M is the most used large dataset for

---

<sup>1</sup>Available at <http://mocap.cs.cmu.edu/>



human motion prediction. CMU contains more sports activities than Human 3.6M, which can help us evaluate the influence of the activities on the adversarial robustness. 3DPW includes various indoor and outdoor activities, which can be used to simulate the real scenario the model needs to face.

**Human3.6M(H3.6M)** has collected 15 types of actions from 7 actors(S1, S5, S6, S7, S8, S9 and S11). The original skeleton in Human3.6M has 32 joints presented by exponential maps. We convert the presentation to 3D coordinates and remove ten redundant joints. The global rotations and translations of poses are excluded. We downsample the frame rate from 50fps to 25fps. S5 and S11 are used for testing and validation, respectively, while other subjects are used for training. In order to compare the results conveniently, we take eight random samples per action for testing.

**CMU-Mocap(CMU)** holds eight categories of actions, with 38 joints presented by exponential maps. We convert the presentation to 3D coordinates as well. The global rotations and translations of poses are excluded too. Following the set in [1], 25 joints in each pose are kept, while the others are excluded. The division of training and testing datasets is also the same as [1]. Like H3.6M, CMU is also sampled into eight random samples per action for testing.

**3DPW(The 3D Pose in the Wild)** contains human motion captured from indoor and outdoor scenes, which are challenging for algorithms. The poses in the dataset are presented in 3D space at 30fps. Each pose contains 24 joints, and 23 joints are used.

### 5.1.2 Baselines

To evaluate the adversarial robustness of the convolution-based models thoroughly, we need to test CNN-based model, GCN-based model, and their derivative methods by our attack method. Therefore we choose LearningTrajectoryDependency [1](LTD), TrajectoryCNN [22] (TrajCNN), HistoryRepeatItself [2] (HRI) and Multi-Head TrajectoryCNN [23](MH TrajCNN).

**LearningTrajectoryDependency** is a representative GCN-based algorithm. LTD first transforms pose information by Discrete Cosine Transform (DCT) to gain a more compact representation and then encodes the spatial structure of human pose by GCNs. Therefore, we need to apply DCT to adversarial samples to make them feasible for LTD.

**TrajectoryCNN** represents a conventional CNN-based baseline that achieves excellent performance. TrajectoryCNN can simultaneously achieve trajectory space transformation, model motion dynamics, and predict future poses by combining the skeletal representation.

**HistoryRepeatItself** enhances the GCN-based structure by utilizing the motion attention mechanism we want to investigate, which can exploit motions instead of static frames to better leverage historical information for motion prediction.

**Multi-Head TrajectoryCNN** can complete the motion prediction task and action recognition task at the same time, which can show whether the proposed attack influences the semantic information of the predicted human motion sequence. Conversely, explicit semantic information modeled by the classification head of Multi-Head TrajectoryCNN may also influence the effectiveness of the proposed attack, which can help us study whether the semantic information is related to the adversarial robustness of human motion prediction models.

Because the target model needs to be a white box, we train our model to be the victim if the official model is not open-sourced, which may cause a difference in the result when we input a clean sequence.

### 5.1.3 Evaluation Metrics

To evaluate the adversarial robustness, we need to calculate how much the predicted motion sequence  $P$  is away from the ground truth  $Y$ . As the result of predicting poses in Cartesian coordinate,

we use Mean Per Joint Position Error (MPJPE), which is defined as the same as Equation (2), to evaluate how much the prediction deviated from the ground truth.

In this work, we are curious how much the adversarial samples against motion prediction can also influence the semantic information of the predicted human motion sequence for action recognition. Therefore, we applied Multi-Head TrajectoryCNN [23], which can complete motion prediction and action recognition at the same time, to verify this hypothesis. When the attack perturbs the motion prediction branch of Multi-Head TrajectoryCNN, we can observe how much the proposed attack influences the performance of the action recognition branch, which indicates whether the proposed attack can be easily detected by normal action recognition. In action recognition, accuracy is used to evaluate the algorithm’s performance; hence we use attack success rate(ASR) to evaluate the attack effectiveness against action recognition. ASR is defined as:

$$ASR = \frac{N_{adv}}{N_{right}} \quad (8)$$

where  $N_{right}$  is the number of clean samples classified correctly, and  $N_{adv}$  is the number of adversarial samples misclassified but classified correctly when clean.

#### 5.1.4 Implementing Details

In our PGD-based attack method, the bound  $\epsilon$  is set from 0.01 to 0.05 with an interval of 0.01, while the step size  $\epsilon_{step}$  is 0.1 times  $\epsilon$ . The iteration number is set to 50. The trade-off parameter  $\lambda$  is set to 0.5. Finally, we attack the whole history human motion sequence in this experiment.

In this work, we train short-term and long-term models separately for LTD and TrajectoryCNN. All the input lengths are set to 10 frames, while their output lengths are set to 10 for short-term prediction and 25 for long-term prediction in Human3.6M and CMU. In 3DPW, the input length is the same as others’ settings, but the output length is set to 15 for short-term and 30 for long-term predictions.

As HRI can effectively make use of motion repetitiveness in long-term history, its input length is set to 50 frames, and its output length is set to 25 frames in Human3.6M and CMU or 30 frames in 3DPW. The attention mechanism in HRI allows it to train a unified model for both short-term and long-term prediction. Thus the HRI model we use will predict ten frames per iteration, three iterations in total, and cut off the prediction sequence. Because our experiment’s datasets differ from Multi-Head TrajectoryCNN’s original setting, we label the motions by the activities in the corresponding dataset and modify Multi-Head TrajectoryCNN’s input into 50 frames and output length into 10 for short-term and 25 frames for long-term to facilitate the comparison.

However, the input length may influence the adversarial robustness of the target models. Therefore, to compare fairly and investigate the impact of the input length, we train LTD and TrajectoryCNN under the same set above, but the input length is changed to 50 frames. We denote them as LTD-50 and TrajCNN-50, respectively. Note that LTD-50 and TrajCNN-50 both contain a short-term and long-term model, which is for a fair comparison with the original models whose input lengths are 10.

## 5.2 Experimental Results

**Human 3.6M** Table 1 and 2 shows the quantitative comparisons of short-term and long-term prediction on Human 3.6M between the above four networks under the attacks of five different intensities (bounds). We blacken the highest error in each time interval of each algorithm and calculate the growth rate from the clean result to the weakest-case and strongest-case result for the convenience of comparison. Due to space limit, detailed tables are provided in the appendix (Table A1-A12).

Table 1: Average prediction errors of target models on Human 3.6M before and after perturbation in variations of the boundary for the models whose input length is 10. The **bold** results are the worst-case of each time interval and the percentage is the least and the most growth rate from the clean error.

Intervals(ms)	80	160	320	400	560	1000
LTD	12.2	25.0	51.0	61.3	78.5	114.3
$\epsilon=0.01$	35.5	73.9	137.4	154.6	184.7	210.5
	(191.0%↑)	(195.6%↑)	(169.4%↑)	(152.2%↑)	(135.3%↑)	(84.2%↑)
$\epsilon=0.02$	45.9	93.0	168.2	187.2	222.1	241.5
$\epsilon=0.03$	53.8	107.6	193.3	214.0	236.2	255.1
$\epsilon=0.04$	56.9	111.2	194.7	213.9	248.3	264.4
$\epsilon=0.05$	<b>60.3</b>	<b>115.7</b>	<b>201.2</b>	<b>220.6</b>	<b>255.6</b>	<b>266.5</b>
	(394.3%↑)	(362.8%↑)	(294.5%↑)	(259.9%↑)	(225.6%↑)	(133.2%↑)
TrajCNN	10.3	23.6	50.3	60.6	78.0	110.6
$\epsilon=0.01$	40.3	93.3	187.2	208.0	199.8	233.8
	(291.3%↑)	(295.3%↑)	(272.2%↑)	(243.2%↑)	(156.2%↑)	(111.4%↑)
$\epsilon=0.02$	58.8	131.8	255.7	280.0	255.8	283.0
$\epsilon=0.03$	68.6	149.7	283.7	308.8	286.8	307.1
$\epsilon=0.04$	72.9	156.3	292.6	317.7	290.8	306.0
$\epsilon=0.05$	<b>77.3</b>	<b>163.7</b>	<b>303.5</b>	<b>328.1</b>	<b>295.8</b>	<b>313.9</b>
	(650.5%↑)	(593.6%↑)	(503.4%↑)	(441.4%↑)	(279.2%↑)	(183.8%↑)

In all cases, even the proposed attack with the minimal  $\epsilon$  achieves significant disturbance (increasing errors by at least 31.2%) to the prediction, proving the attack’s effectiveness and the current models’ vulnerability. These results mean the proposed attack can find the worst-case adversarial examples for each model, which can thoroughly analyze the adversarial robustness of the target models. However, the attack effectiveness will be weakened as the time interval grows. This weakening phenomenon may attribute to the limited space where poses are set and the excellent comprehension of the target models to the human motion, which doesn’t allow the predicted motion to perform impossible activities.

Comparing the results of each model, the model with a lower growth rate of prediction errors is more adversarial robust, which means the model can maintain its normal prediction ability and resist attack effectiveness. Therefore, LTD-50 is the most adversarial robust, then LTD, MH TrajCNN, HRI, TrajCNN, and TrajCNN-50 are the most vulnerable. These results show that the excellent performance of the human motion prediction algorithm in the clean circumstance is not related to its adversarial robustness.

In light of our observation, prior knowledge and semantic information are key to the adversarial robustness of human motion prediction. According to the rank above, the GCN-based structure is more adversarial robust than the CNN structure. The adjacent matrices in GCN provide prior knowledge of human pose and constrain the model during the inference stage, which can suppress the disturbance from the proposed attack. Thus, the adversarial robustness of LTD comes out in front. Without constraints like graphs, the CNN-based structure has little resistance against the adversarial attack. Nevertheless, the semantic information modeled explicitly in MH TrajCNN enhances its adversarial robustness. MH TrajCNN can keep the error low when facing weak attacks but can’t withstand intense attacks, which still enlarge the errors.

Comparing the errors of LTD and LTD-50 or TrajCNN and TrajCNN-50, the length of input frames is also a significant factor for human motion prediction models. Except for TrajCNN with a large  $\epsilon$ , the errors and the growth rates when the input length is 50 are obviously lower than those when the input length is 10, and a large margin decreases the errors of repetitive activities like Walking. The reason input length influences the adversarial robustness may be that longer human motion sequences help the models learn better about the kinematics of the human body, especially the repetitive information. Nevertheless, increasing input length is a rapier for adversarial robustness because when the parameter quantity of the input data is enlarged, the chance for the adversary to attack is also increased. The results of TrajCNN when  $\epsilon$  is 0.05 show that increasing input length is not always valid, and the disturbance of the attack can burst when the attack is intense enough.

However, comparing the results between HRI and LTD-50, the attention mechanism is a burden

Table 2: Average prediction errors of target models on Human 3.6M before and after perturbation in boundary variations for the models whose input length is 50. The **bold** results are the worst-case of each time interval, and the percentage is the least and the most growth rate from the clean error.

Intervals(ms)	80	160	320	400	560	1000
LTD-50	13.8	27.8	54.3	66.7	87.4	116.7
$\epsilon=0.01$	26.7	50.5	87.8	100.8	140.3	169.1
	(93.5% $\uparrow$ )	(81.7% $\uparrow$ )	(61.7% $\uparrow$ )	(51.1% $\uparrow$ )	(60.5% $\uparrow$ )	(44.9% $\uparrow$ )
$\epsilon=0.02$	34.0	65.8	115.0	128.7	177.0	204.1
$\epsilon=0.03$	41.7	81.9	143.9	158.2	200.9	224.8
$\epsilon=0.04$	48.8	96.0	169.5	185.5	216.9	238.2
$\epsilon=0.05$	<b>52.2</b>	<b>101.3</b>	<b>175.9</b>	<b>192.0</b>	<b>232.8</b>	<b>250.8</b>
	(278.3% $\uparrow$ )	(264.4% $\uparrow$ )	(223.9% $\uparrow$ )	(187.9% $\uparrow$ )	(166.4% $\uparrow$ )	(114.9% $\uparrow$ )
TrajCNN-50	10.0	22.5	46.3	58.6	80.0	110.1
$\epsilon=0.01$	36.1	82.5	168.9	193.3	154.0	185.4
	(261.0% $\uparrow$ )	(266.7% $\uparrow$ )	(264.8% $\uparrow$ )	(229.9% $\uparrow$ )	(92.5% $\uparrow$ )	(68.4% $\uparrow$ )
$\epsilon=0.02$	55.8	122.8	241.6	271.1	225.3	247.4
$\epsilon=0.03$	69.7	149.2	286.2	317.5	275.1	292.2
$\epsilon=0.04$	80.3	167.8	315.9	347.6	319.3	333.8
$\epsilon=0.05$	<b>92.0</b>	<b>188.9</b>	<b>350.1</b>	<b>382.9</b>	<b>356.5</b>	<b>371.3</b>
	(820.0% $\uparrow$ )	(739.6% $\uparrow$ )	(756.2% $\uparrow$ )	(653.4% $\uparrow$ )	(345.6% $\uparrow$ )	(237.2% $\uparrow$ )
HRI	10.4	22.6	47.1	58.3	77.3	112.1
$\epsilon=0.01$	33.6	75.9	153.9	178.2	201.0	209.4
	(223.1% $\uparrow$ )	(235.8% $\uparrow$ )	(226.8% $\uparrow$ )	(205.7% $\uparrow$ )	(160.0% $\uparrow$ )	(86.8% $\uparrow$ )
$\epsilon=0.02$	46.6	100.5	194.4	221.1	243.3	244.8
$\epsilon=0.03$	57.5	119.7	223.6	250.9	270.9	265.6
$\epsilon=0.04$	65.7	133.0	242.3	270.4	290.0	281.5
$\epsilon=0.05$	<b>72.0</b>	<b>142.4</b>	<b>254.3</b>	<b>281.9</b>	<b>300.3</b>	<b>288.4</b>
	(592.3% $\uparrow$ )	(530.1% $\uparrow$ )	(439.9% $\uparrow$ )	(383.5% $\uparrow$ )	(288.5% $\uparrow$ )	(157.3% $\uparrow$ )
MH TrajCNN	12.1	26.4	52.7	65.5	84.7	113.3
$\epsilon=0.01$	27.3	53.5	96.4	110.3	121.2	148.7
	(125.6% $\uparrow$ )	(102.7% $\uparrow$ )	(82.9% $\uparrow$ )	(68.4% $\uparrow$ )	(43.1% $\uparrow$ )	(31.2% $\uparrow$ )
$\epsilon=0.02$	46.1	88.1	153.6	170.5	172.0	195.4
$\epsilon=0.03$	61.6	114.6	193.1	211.6	217.6	237.3
$\epsilon=0.04$	76.4	140.9	233.9	253.7	250.1	264.5
$\epsilon=0.05$	<b>89.2</b>	<b>161.0</b>	<b>260.4</b>	<b>279.4</b>	<b>277.4</b>	<b>288.7</b>
	(637.2% $\uparrow$ )	(509.8% $\uparrow$ )	(394.1% $\uparrow$ )	(326.6% $\uparrow$ )	(227.5% $\uparrow$ )	(154.8% $\uparrow$ )

under attack for human motion prediction. The attention mechanism can help HRI learn the different sub-sequence contributions and the repetitive pattern of the input human motion sequence. The proposed attack can mislead the attention and enlarge the disturbance caused by the perturbed parts of the human motion sequence. To our surprise, in Human 3.6M, the augmentation used in HRI for the history motion sequence with the last prediction does not cause a further influence on the attack effectiveness, which may be because the original history human motion sequence takes the upper hand in the augmented history human motion sequence.

Most of the absolute average errors increased as the time interval enlarged, but the errors of TrajCNN and HRI don't follow this trend in long-term prediction. The reason for this non-monotonic phenomenon is different for the two models. For TrajCNN, we attribute this phenomenon to the short- to long-term switching model. These two models may use different ways to deal with the perturbed input. For HRI, this phenomenon may attribute to the attention mechanism, which gives HRI efficiency in capturing repetitiveness. As we only maximize the average prediction error, it is hard to ensure the specific errors in each time interval, especially for repetitive activities. This phenomenon only happens when  $\epsilon$  is larger than 0.02, and the motion is more and more out of the control of the clean sequence when  $\epsilon$  is larger and larger. According to our observation, the perturbed prediction motions hardly repeat in pattern, which makes it possible for the joints in repetitive motions to move close to the ground truth location when the time interval is large enough. As a result, the non-monotonic phenomenon occurs in HRI. This non-monotonic phenomenon is more frequent in specific activities and will be discussed in the appendix due to space limits.

CMU-Mocap Table 3 and 4 shows the error comparisons of the target models on CMU-Mocap, and the detailed tables are in the appendix (Table A13-A24). On this dataset, the target models are also severely interrupted. However, the most adversarial robust algorithm is LTD-50, LTD, then MH TrajCNN, TrajCNN, TrajCNN-50, and finally, HRI is the most vulnerable model.

CMU-Mocap contains more sports activities, which causes the difference in the attack effectiveness

Table 3: Average prediction errors of target models on CMU before and after perturbation in boundary variations for the models whose input length is 10. The **bold** results are the worst-case of each time interval, and the percentage is the least and the most growth rate from the clean error.

Intervals(ms)	80	160	320	400	560	1000
LTD	10.1	18.0	36.3	46.8	62.7	95.0
$\epsilon=0.01$	20.9	41.1	86.1	107.5	140.9	181.0
	(106.9% $\uparrow$ )	(128.3% $\uparrow$ )	(137.2% $\uparrow$ )	(129.7% $\uparrow$ )	(124.7% $\uparrow$ )	(90.5% $\uparrow$ )
$\epsilon=0.02$	29.6	56.5	114.7	141.5	173.0	211.1
$\epsilon=0.03$	35.9	66.6	133.1	163.4	193.0	230.4
$\epsilon=0.04$	39.7	71.9	140.8	171.7	203.7	242.0
$\epsilon=0.05$	<b>43.5</b>	<b>76.3</b>	<b>146.1</b>	<b>177.5</b>	<b>209.0</b>	<b>245.8</b>
	(330.7% $\uparrow$ )	(323.9% $\uparrow$ )	(302.5% $\uparrow$ )	(279.3% $\uparrow$ )	(233.3% $\uparrow$ )	(158.7% $\uparrow$ )
TrajCNN	8.4	15.2	32.4	42.5	60.7	94.0
$\epsilon=0.01$	22.0	43.4	94.3	118.7	128.7	185.3
	(161.9% $\uparrow$ )	(185.5% $\uparrow$ )	(191.0% $\uparrow$ )	(179.3% $\uparrow$ )	(112.0% $\uparrow$ )	(97.1% $\uparrow$ )
$\epsilon=0.02$	33.5	65.0	136.4	169.3	179.2	243.8
$\epsilon=0.03$	42.9	80.8	164.9	202.6	207.6	274.3
$\epsilon=0.04$	48.6	90.4	181.5	221.7	224.4	291.1
$\epsilon=0.05$	<b>54.3</b>	<b>98.1</b>	<b>191.8</b>	<b>232.2</b>	<b>238.7</b>	<b>307.1</b>
	(546.4% $\uparrow$ )	(545.4% $\uparrow$ )	(492.0% $\uparrow$ )	(446.4% $\uparrow$ )	(293.2% $\uparrow$ )	(226.7% $\uparrow$ )

and the adversarial robustness rank. Comparing the errors between Human 3.6M and CMU, the growth rates in CMU are much less than those in Human 3.6M. This result shows that the activities with more movements may cause the attack effectiveness to be weaker, or the model trained with a specialized kind of activity may be more adversarial robust.

However, surpassed by TrajCNN, HRI drops to the last place in the ranking of adversarial robustness, which may attribute to the attention mechanism and the augmentation with the last prediction. The misleading effect comes into force to HRI as it does in the Human 3.6M and is noticeable when predicting the “running” activity in CMU. For the activities in CMU, the augmentation in HRI stabilizes the attack effectiveness as the prediction time interval grows. Note that the kernel size of HRI is 10, which means 80ms, 160ms, 320ms, and 400ms are in the first window, 560ms is in the second window, and 1000ms is in the third window. The attack against other target models will weaken as the time interval is enlarged, while the attack effectiveness against HRI decreases much slower. Comparing the long-term results between LTD-50 and HRI, it is clear that the errors of HRI in 560ms and 1000ms increase much faster than those of LTD-50. Therefore, the last prediction used to augment the history motion sequence has more influence when the model focuses on sports activities.

**3DPW** Table 5 and 6 shows the comparisons on 3DPW. The proposed attack still works well against all the target models. Based on the error growth rates, the models can be generally sorted from robust to vulnerable as LTD-50, LTD, TrajCNN-50, TrajCNN, and HRI. The activities from 3DPW are wilder than the other two datasets. Thus, the average results shows more features of the complex activities.

One of the reasons why the growth rate of the errors under attack is relatively low is that the activities in 3DPW are wilder than those in CMU. As the results in CMU show that activities with more movements can weaken the attack, the attack effectiveness judged from the growth rates in 3DPW is not as drastic as in other datasets. Although another reason is that the errors under the clean circumstance are much higher than those in Human 3.6M and CMU, most of the absolute errors of the same time interval in 3DPW are lower, proving the influence of the complexity on the attack.

**Semantic Information** With the help from the classification branch of MH TrajCNN, we can observe whether the proposed attack influences the semantic information of the predicted sequence based on the ASR results. As shown in Table 7, most of the ASR is at a low level, which indicates that the proposed attack has little effect on the semantic information of the predicted sequence.

However, the long-term classifier in Human 3.6M and the short-term classifier in CMU are more sensitive than the others as their ASRs are relatively higher. The reason may be the different composition of the activities in these two datasets. The activities in Human 3.6M are more than in CMU in amount and variety. Moreover, there are more static activities in Human 3.6M, while most of the activities in

Table 4: Average prediction errors of target models on CMU before and after perturbation in boundary variations for the models whose input length is 50. The **bold** results are the worst-case of each time interval, and the percentage is the least and the most growth rate from the clean error.

Intervals(ms)	80	160	320	400	560	1000
LTD-50	9.3	17.0	33.9	43.1	63.0	94.3
$\epsilon=0.01$	21.8	40.4	78.5	92.2	113.7	152.4
	(134.4% $\uparrow$ )	(137.6% $\uparrow$ )	(131.6% $\uparrow$ )	(113.9% $\uparrow$ )	(80.5% $\uparrow$ )	(61.6% $\uparrow$ )
$\epsilon=0.02$	27.6	51.9	102.9	119.9	140.5	177.1
$\epsilon=0.03$	32.2	59.2	116.1	134.5	159.9	195.7
$\epsilon=0.04$	37.2	67.8	132.9	153.5	180.1	215.0
$\epsilon=0.05$	<b>41.2</b>	<b>73.6</b>	<b>140.7</b>	<b>161.3</b>	<b>194.4</b>	<b>229.5</b>
	(343.0% $\uparrow$ )	(332.9% $\uparrow$ )	(315.0% $\uparrow$ )	(274.2% $\uparrow$ )	(208.6% $\uparrow$ )	(143.4% $\uparrow$ )
TrajCNN-50	8.8	16.4	33.5	43.3	61.7	97.3
$\epsilon=0.01$	20.4	39.9	83.0	103.6	102.9	144.7
	(131.8% $\uparrow$ )	(143.3% $\uparrow$ )	(147.8% $\uparrow$ )	(139.3% $\uparrow$ )	(66.8% $\uparrow$ )	(48.7% $\uparrow$ )
$\epsilon=0.02$	32.4	62.4	126.9	155.9	154.7	203.2
$\epsilon=0.03$	42.3	79.3	156.2	189.5	198.7	248.2
$\epsilon=0.04$	52.1	95.8	183.8	219.9	232.9	277.8
$\epsilon=0.05$	<b>59.8</b>	<b>108.5</b>	<b>207.7</b>	<b>249.0</b>	<b>249.1</b>	<b>293.8</b>
	(579.5% $\uparrow$ )	(561.6% $\uparrow$ )	(620.0% $\uparrow$ )	(475.1% $\uparrow$ )	(303.7% $\uparrow$ )	(302.0% $\uparrow$ )
HRI	9.5	17.0	33.9	43.2	59.8	101.6
$\epsilon=0.01$	22.6	48.1	114.5	148.8	210.8	285.8
	(137.9% $\uparrow$ )	(182.9% $\uparrow$ )	(237.8% $\uparrow$ )	(244.4% $\uparrow$ )	(252.5% $\uparrow$ )	(181.3% $\uparrow$ )
$\epsilon=0.02$	34.1	70.6	159.0	202.9	273.8	335.5
$\epsilon=0.03$	42.1	83.6	182.1	230.0	305.0	367.4
$\epsilon=0.04$	48.6	93.3	196.5	245.8	319.0	377.4
$\epsilon=0.05$	<b>55.3</b>	<b>104.1</b>	<b>215.9</b>	<b>268.6</b>	<b>344.4</b>	<b>397.4</b>
	(482.1% $\uparrow$ )	(512.4% $\uparrow$ )	(536.9% $\uparrow$ )	(521.8% $\uparrow$ )	(475.9% $\uparrow$ )	(291.1% $\uparrow$ )
MH TrajCNN	9.7	17.7	36.9	47.5	68.4	103.3
$\epsilon=0.01$	16.8	29.0	56.2	69.3	93.8	130.3
	(73.2% $\uparrow$ )	(63.8% $\uparrow$ )	(52.3% $\uparrow$ )	(45.9% $\uparrow$ )	(37.1% $\uparrow$ )	(26.1% $\uparrow$ )
$\epsilon=0.02$	26.1	43.5	80.7	97.7	127.0	169.1
$\epsilon=0.03$	36.0	59.6	108.9	131.1	164.4	214.7
$\epsilon=0.04$	45.8	74.4	133.5	159.4	194.9	244.9
$\epsilon=0.05$	<b>54.4</b>	<b>86.7</b>	<b>151.6</b>	<b>179.4</b>	<b>220.7</b>	<b>269.1</b>
	(460.8% $\uparrow$ )	(389.8% $\uparrow$ )	(310.8% $\uparrow$ )	(277.7% $\uparrow$ )	(222.7% $\uparrow$ )	(160.5% $\uparrow$ )

CMU are from sports. Hence the semantic information learned from Human 3.6M may focus more on the detailed information, which makes the classification branch trained in the long-term model on Human 3.6M more sensitive. Meanwhile, distinguishing motions with high frequency is more common in CMU for the classification branch in MH TrajCNN, making the classifier focus more on the pattern information that needs to be expected for a longer time.

Considering the results in Table 7 and comparing the short-term and long-term MH TrajCNN errors, the MH TrajCNN with a more sensitive classifier suppresses the attack effectiveness less than the others when facing the proposed attack with  $\epsilon = 0.05$ . This phenomenon indicates the sensitivity of the classification branch may negatively relate to the influence of the semantic information modeling on the adversarial robustness of the model when the model is facing an intense attack.

**Qualitative Results** The qualitative results prove the stealthiness of the proposed attack. When

Table 5: Average prediction errors of target models on 3DPW before and after perturbation in boundary variations for the models whose input length is 10. The **bold** results are the worst-case of each time interval, and the percentage is the least and the most growth rate from the clean error.

Intervals(ms)	200	400	600	800	1000
LTD	34.4	65.7	93.6	105.6	113.5
$\epsilon=0.01$	56.3	103.9	181.6	205.7	211.0
	(63.7% $\uparrow$ )	(58.1% $\uparrow$ )	(94.0% $\uparrow$ )	(94.8% $\uparrow$ )	(85.9% $\uparrow$ )
$\epsilon=0.02$	68.8	125.0	209.8	236.0	240.1
$\epsilon=0.03$	77.6	138.8	221.9	248.7	252.1
$\epsilon=0.04$	83.6	147.4	227.6	254.4	257.3
$\epsilon=0.05$	<b>88.3</b>	<b>153.4</b>	<b>231.0</b>	<b>257.8</b>	<b>260.3</b>
	(156.7% $\uparrow$ )	(133.5% $\uparrow$ )	(146.8% $\uparrow$ )	(144.1% $\uparrow$ )	(129.3% $\uparrow$ )
TrajCNN	29.9	60.0	85.3	99.3	107.5
$\epsilon=0.01$	66.3	129.2	132.7	147.3	150.3
	(121.7% $\uparrow$ )	(115.3% $\uparrow$ )	(55.6% $\uparrow$ )	(48.3% $\uparrow$ )	(39.8% $\uparrow$ )
$\epsilon=0.02$	96.7	179.2	168.8	182.1	181.9
$\epsilon=0.03$	116.7	209.0	191.5	202.9	200.9
$\epsilon=0.04$	128.7	225.9	204.8	214.8	212.1
$\epsilon=0.05$	<b>137.1</b>	<b>237.0</b>	<b>214.0</b>	<b>223.0</b>	<b>219.8</b>
	(358.5% $\uparrow$ )	(295.0% $\uparrow$ )	(150.9% $\uparrow$ )	(124.6% $\uparrow$ )	(104.5% $\uparrow$ )

Table 6: Average prediction errors of target models on 3DPW before and after perturbation in boundary variations for the models whose input length is 10. The **bold** results are the worst-case of each time interval, and the percentage is the least and the most growth rate from the clean error.

Intervals(ms)	200	400	600	800	1000
LTD-50	34.8	65.1	93.1	104.9	113.5
$\epsilon=0.01$	54.3 (56.0% $\uparrow$ )	91.8 (41.0% $\uparrow$ )	131.2 (40.9% $\uparrow$ )	144.4 (37.7% $\uparrow$ )	153.0 (34.8% $\uparrow$ )
$\epsilon=0.02$	63.2	108.5	158.1	172.0	180.9
$\epsilon=0.03$	70.1	120.7	174.7	188.9	197.8
$\epsilon=0.04$	75.8	130.0	186.0	200.2	209.2
$\epsilon=0.05$	<b>80.6</b> (131.6% $\uparrow$ )	<b>137.5</b> (111.2% $\uparrow$ )	<b>194.2</b> (108.6% $\uparrow$ )	<b>208.5</b> (98.8% $\uparrow$ )	<b>217.5</b> (91.6% $\uparrow$ )
TrajCNN-50	31.1	61.4	86.2	101.1	111.2
$\epsilon=0.01$	58.6 (88.4% $\uparrow$ )	109.0 (77.5% $\uparrow$ )	114.7 (33.1% $\uparrow$ )	129.8 (28.4% $\uparrow$ )	136.1 (22.4% $\uparrow$ )
$\epsilon=0.02$	90.8	161.3	148.1	162.3	165.2
$\epsilon=0.03$	119.2	203.6	177.8	190.2	190.1
$\epsilon=0.04$	142.6	235.8	202.1	212.2	209.7
$\epsilon=0.05$	<b>161.7</b> (419.9% $\uparrow$ )	<b>260.3</b> (323.9% $\uparrow$ )	<b>221.4</b> (156.8% $\uparrow$ )	<b>229.3</b> (126.8% $\uparrow$ )	<b>224.8</b> (102.2% $\uparrow$ )
HRI	43.1	85.9	114.6	133.6	146.8
$\epsilon=0.01$	98.6 (128.8% $\uparrow$ )	185.9 (116.4% $\uparrow$ )	228.0 (99.0% $\uparrow$ )	244.4 (82.9% $\uparrow$ )	247.5 (68.6% $\uparrow$ )
$\epsilon=0.02$	128.1	232.3	275.9	288.3	287.1
$\epsilon=0.03$	145.6	257.8	300.7	310.7	307.6
$\epsilon=0.04$	158.3	275.1	317.4	325.5	321.0
$\epsilon=0.05$	<b>167.5</b> (288.6% $\uparrow$ )	<b>287.2</b> (234.3% $\uparrow$ )	<b>329.0</b> (187.1% $\uparrow$ )	<b>336.0</b> (151.5% $\uparrow$ )	<b>330.9</b> (125.4% $\uparrow$ )

Table 7: Accuracy and ASR of short-term and long-term Multi-Head TrajectoryCNN on H3.6M and CMU before and after perturbation in different boundaries.

	clean	$\epsilon=0.01$	$\epsilon=0.02$	$\epsilon=0.03$	$\epsilon=0.04$	$\epsilon=0.05$
Human 3.6m						
Accuracy-short	63.3%	62.5%	62.5%	65.0%	60.8%	60.0%
ASR-short	-	1.3%	2.7%	2.7%	10.7%	10.7%
Accuracy-long	58.3%	56.7%	55.8%	55.0%	55.0%	50.0%
ASR-long	-	2.9%	4.3%	8.6%	10.0%	18.6%
CMU						
Accuracy-short	82.8%	79.7%	78.1%	76.6%	68.8%	68.8%
ASR-short	-	3.8%	5.7%	7.5%	17.0%	17.0%
Accuracy-long	82.8%	81.3%	79.7%	78.1%	78.1%	75.0%
ASR-long	-	1.9%	3.8%	5.7%	5.7%	9.4%

every input pose is listed on the left side of Figure 2, it is easy to find that the perturbations hardly change the input human motion sequences visually. On the contrary, the predicted poses shown on the right side of Figure 2 are significantly misled far away from the ground truth, indicating the proposed attack’s effectiveness.

The differences between the clean human motion sequence and the perturbed motion sequence are so tiny that it is hard to distinguish most parts in these two sequences when overlapping them. Therefore, we use red boxes to mark the poses with noticeable visual differences. According to the red boxes, the perturbation tends to modify the last frame of the input more than other frames. This tendency is not only happening to LTD but happening to all target models. The reason can be summarized as follows: 1) The last frame strongly correlates to predicting human motion, which means the last frame can define most of the information in the following motion, e.g., directions. Thus, the optimization for attack takes more weight on the last frame. 2) In LTD and TrajCNN, the last frame is regarded as the observed pose and repeats  $T_f$  times, emphasizing the last frame in the optimization.

Although the perturbed sequence is difficult to be noticed when every frame is picked, the perturbation is easier to be noticed when the perturbed human motion sequence is made into animation like GIF. Based on our observation, the perturbed motion looks like shaking, while its predicted motion will suddenly be bizarre, including making actions impossible for humans and falling like an offline puppet.



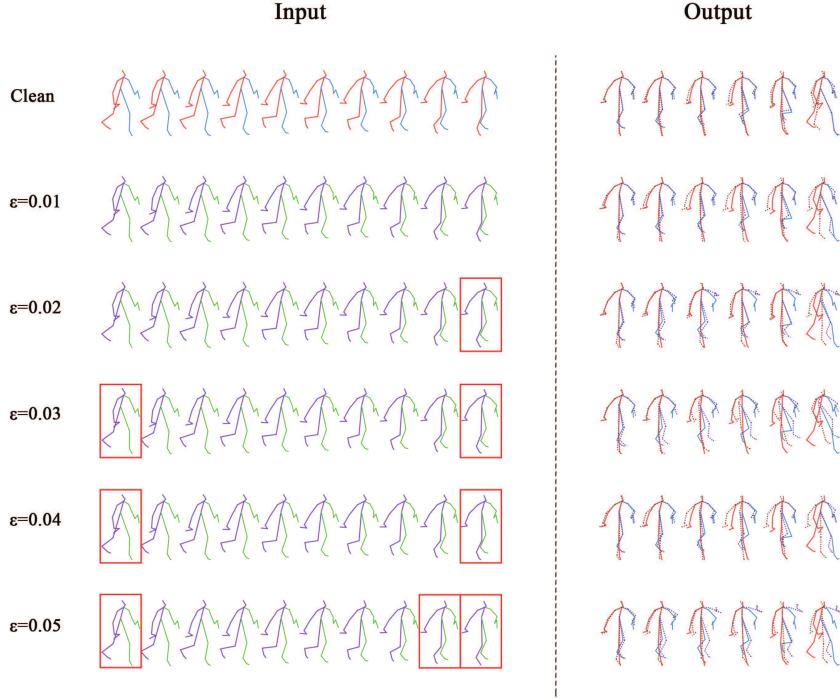


Figure 2: This figure shows LTD’s prediction result of “walking” before and after the attack. The poses with solid lines in red and blue are the clean input and ground truth; For the input sequences, the skeletons in purple and green are the perturbed sequence under the attack with the corresponding intensities written on the left. As for the output sequences, the dotted skeletons in the prediction are the predicted poses when their time intervals are 80ms, 160ms, 320ms, 400ms, 560ms, and 1000ms. Because the differences between the clean input and the perturbed input are tiny, we mark the poses with relatively noticeable changes with red boxes.

## 6 Ablation Study

### 6.1 Scale Function

The scale function in the proposed scheme can help the attack method find a proper unit of length automatically without considering the scale parameter of the collecting equipment, which the results in Table 8 can prove. In this study, we remove the scale function, use a fixed parameter  $\epsilon_{fix}$  as the boundary and its 0.1 times as the step size, and achieve a set of similar errors as the results when we apply the scale function and set  $\epsilon = 0.01$ . The study is all against the long-term LTD on each dataset. Besides the boundary and the step size, the proposed attack method has no more change.

According to the results in Table 8, the scale function can adapt to the scale parameter of the equipment. To determine the value of the boundary  $\epsilon_{fix}$ , we calculate each dataset’s average outcomes of the scale function. The approximate values are 329.5 for Human 3.6M, 403.0 for CMU, and 0.3 for 3DPW. As the boundary is the product of 0.01 and the calculated scale,  $\epsilon_{fix}$  are 3, 4, 0.003 for Human

Table 8: The similar attack effectiveness against LTD using the fixed boundaries or the scale function in the proposed scheme. The fixed boundaries  $\varepsilon_{fix}$  are various and determined by the product of 0.01 and the average scales calculated by the proposed function, which is the same as the experiment setting when  $\varepsilon=0.01$ . This result proves that the proposed function can handle the scale variance among different equipment and adapt to different activities, enhancing the attack’s stealthiness.

Human 3.6M						
Intervals(ms)	80	160	320	400	560	1000
Scale( $\varepsilon=0.01$ )	33.7	69.9	136.3	159.7	187.4	212.6
$\varepsilon_{fix}=3.0$	32.7	68.1	133.6	157.0	185.1	211.3
CMU						
Intervals(ms)	80	160	320	400	560	1000
Scale( $\varepsilon=0.01$ )	20.9	39.5	82.6	104.1	140.7	180.4
$\varepsilon_{fix}=4.0$	21.1	39.8	83.3	105.3	142.9	184.5
3DPW						
Intervals(ms)	200	400	600	800	1000	
Scale( $\varepsilon=0.01$ )	72.2	138.0	182.0	206.1	211.4	
$\varepsilon_{fix}=0.003$	73.3	140.4	185.4	210.0	215.3	

3.6M, CMU, 3DPW, respectively. Note that the length unit of Human 3.6M, and CMU is a meter, while the unit of 3DPW is a millimeter. Thus, the scale of 3DPW is much different from the others. In the actual scenario, the adversary may not know the scale parameter. Suppose the adversary attacks the human motion data with an inappropriate scale. In that case, the perturbed motion sequence will have a weak attack effectiveness or the perturbed motion will be crushed into a mess. These are the situations we do not want the proposed attack meets. For the proposed scale function, the scale of the motion sequence is calculated in advance, and the adversary can directly attack the model in a uniform parameter setting, which solves the problem of unknown scale parameters.

Comparing the  $\varepsilon_{fix}$  of Human 3.6M and CMU, the scale function can also adapt to the range of the input motion. CMU contains more vigorous activities than Human 3.6M does. Thus, the average scale of CMU is larger than Human 3.6M. This operation can enhance the effectiveness of the proposed attack while ensuring its stealthiness at the same time. Human perception is based on relative relations, which means humans can tolerate a more significant perturbation in a more vigorous motion. Nevertheless, a small perturbation may be easily found in slow motion.

Although the  $\varepsilon_{fix}$  is determined by the average scale calculated by the proposed function, the errors when using fixed boundary on CMU and 3DPW are obviously higher than when using the scale function. The scale function aims to find basic length units suitable for the input motion sequences. Hence, the outcomes can be various. The mean cannot reflect the position of most scales, and some activities with high scales in CMU and 3DPW lift the mean of the scales. In such circumstance, most of the activities with lower scales are attacked by the proposed attack but with a larger boundary, which cause the difference between using fixed boundaries and using the scale function.

## 6.2 Vulnerability of each frame

To discover the vulnerability of different frames in the input sequence, we divide the input sequence into four parts: *front*, *middle*, *rear*, and *last*, as shown in Figure 3. For TrajCNN and LTD, which input 10 frames, Without the *last* frame, the input sequence contains nine frames that can be separated into three equal parts: *front*, *middle*, and *rear*. For HRI, which inputs 50 frames, we set the last two input frames as the *last* part and then segment the rest of the frames into the rest three parts. In this experiment, we set  $\varepsilon$  to 0.01 and attack the long-term models we train. During the optimization, we mask all frames but the frames in the part we attack, and the results are shown in Table 9.

The vulnerability of the frame increases as the frame gets closer to the observed frame. Compared to the apparent attack effectiveness of the latter two parts, attacking the *front* and *middle* parts can hardly disturb the prediction. Furthermore, attacking the *last* frame sometimes is even more effective than the

Table 9: The comparison of average prediction errors when we perturb different positions of the input sequence. The bold results are the worst-case of each time interval.

Intervals(ms)	80	160	320	400	560	1000
LTD	13.5	26.8	51.9	62.0	78.5	114.3
LTD(front)	15.2	29.4	54.5	64.5	80.7	116.3
LTD(middle)	15.3	29.5	54.8	64.9	81.1	116.6
LTD(rear)	21.8	<b>46.5</b>	<b>92.4</b>	<b>109.4</b>	<b>132.5</b>	162.9
LTD(last)	<b>22.8</b>	45.1	87.2	104.1	128.7	<b>163.6</b>
TrajCNN	11.7	26.0	52.5	62.4	78.0	110.6
TrajCNN(front)	11.7	26.0	52.6	62.5	78.2	110.8
TrajCNN(middle)	11.7	26.0	52.6	62.5	78.2	110.8
TrajCNN(rear)	18.1	41.0	<b>87.0</b>	<b>104.9</b>	<b>131.5</b>	165.8
TrajCNN(last)	<b>20.3</b>	<b>41.1</b>	84.1	102.2	130.6	<b>166.3</b>
HRI	10.4	22.6	47.1	58.3	77.3	112.1
HRI(front)	11.3	24.1	49.9	60.8	78.4	112.9
HRI(middle)	11.3	24.1	49.9	60.7	78.3	112.9
HRI(rear)	12.8	28.6	60.8	73.9	93.1	124.8
HRI(last)	<b>28.9</b>	<b>64.6</b>	<b>132.4</b>	<b>155.3</b>	<b>178.9</b>	<b>191.6</b>

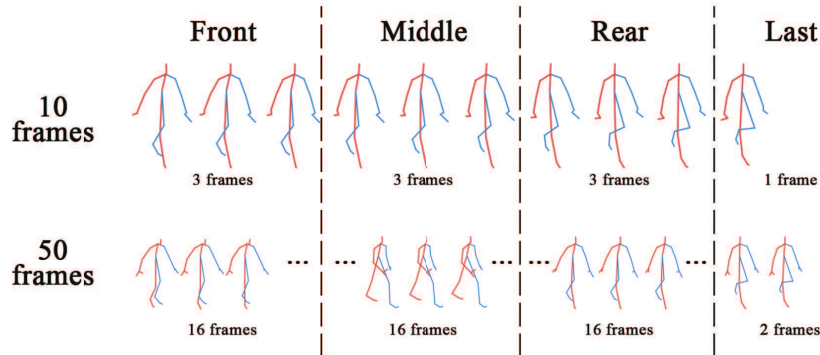


Figure 3: This figure shows how to divide the input human motion sequence into the *front*, *middle*, *rear*, and *last* parts when the input length is 10 or 50 frames. The number of frames in each part is written under the poses of the corresponding parts.

*rear* frames. The result is clear that the *rear* and *last* frames are more vulnerable than the *front* and *middle* frames, which means the closer a frame is to the observed frame, the stronger attack effectiveness it may generate. Especially the observed frame is the most important to the adversarial robustness of human motion prediction models, which corresponds to the observation that the last frame takes more weight during the optimization.

For LTD and TrajCNN, some activities show that attacking the *rear* part of these activities gives more boost to the disturbance than attacking the *last* part. The reason may be that the frames before the observed frame contribute more pattern information of the human motion. Only perturbing the *last* frame gives momentum to lead the move away, but the remaining parts of the sequence are correct, which may partly remedy the prediction. The thought is also supported by the observation that the sum of increasing amounts when perturbing different parts is lower than the increasing amounts when perturbing the whole input generates.

However, HRI may pay more attention to the *last* part because the errors when attacking the *last* part are much higher than the errors when attacking the other parts. Although attacking the *rear* part is relatively more effective than attacking the *front* and *middle* parts, attacking these three parts results in similar errors, which means there is almost no attack effectiveness. Note that the *last* part of HRI's input is the last two frames, which can contain more motion information than the last frame. Still, this

phenomenon is exaggerated for a model that can make use of motion repetitiveness, which also means the contribution of the *last* part is much more than the rest of the frames.

### 6.3 Effect of Physical Constraints

Table 10: The comparison of average prediction errors on Human 3.6M when the attack is under different constraints.  $\overline{\Delta BL}$  is the average absolute change per bone in the whole test set.  $\overline{\Delta V}$  and  $\overline{\Delta a}$  are the average absolute change per joint of velocity and acceleration in the whole test. The bold results are the highest errors in each time interval and the smallest changes in  $\overline{\Delta BL}$ ,  $\overline{\Delta V}$ , and  $\overline{\Delta a}$ , which indicates the best attack effectiveness and the best stealthiness.

Intervals(ms)	80	160	320	400	560	1000	$\overline{\Delta BL}$	$\overline{\Delta V}$	$\overline{\Delta a}$
LTD	13.5	26.8	51.9	62.0	78.5	114.3	-	-	-
LTD(no constraint)	<b>42.8</b>	<b>90.9</b>	<b>180.9</b>	<b>212.6</b>	<b>248.5</b>	<b>267.7</b>	2.67	6.07	8.86
LTD(temporal constraint)	37.6	77.9	150.8	175.6	204.4	224.4	1.41	1.17	1.10
LTD(bone-length constraint)	36.6	76.8	150.9	177.1	207.8	232.5	1.08	3.45	4.41
LTD(both constraints)	33.1	68.5	133.6	156.8	184.7	210.5	<b>1.00</b>	<b>1.08</b>	<b>1.08</b>
TrajCNN	11.7	26.0	52.5	62.4	78.0	110.6	-	-	-
TrajCNN(no constraint)	<b>34.7</b>	<b>76.1</b>	<b>164.1</b>	<b>200.2</b>	<b>249.4</b>	<b>284.6</b>	2.67	7.52	10.82
TrajCNN(temporal constraint)	31.5	66.9	141.4	172.2	215.5	249.6	1.67	1.43	1.12
TrajCNN(bone-length constraint)	32.0	69.1	146.6	178.4	223.8	259.9	0.42	4.17	5.03
TrajCNN(both constraints)	29.7	63.2	132.2	160.1	199.8	233.8	<b>0.40</b>	<b>1.30</b>	<b>1.10</b>
HRI	10.4	22.6	47.1	58.3	77.3	112.1	-	-	-
HRI(no constraint)	<b>39.9</b>	<b>92.3</b>	<b>189.1</b>	<b>218.4</b>	<b>244.6</b>	<b>248.7</b>	2.60	3.26	5.78
HRI(temporal constraint)	35.4	79.8	161.9	187.4	210.8	217.6	0.62	1.02	<b>1.40</b>
HRI(bone-length constraint)	35.7	81.0	164.1	190.0	213.6	220.6	0.35	2.74	4.43
HRI(both constraints)	33.6	75.9	153.9	178.2	201.0	209.4	<b>0.32</b>	<b>0.96</b>	1.41

To investigate the effect of the proposed physical constraints on the attack effectiveness and imperceptibility, we compare the attack under different constraints on Human 3.6M. In this section, we use  $\overline{\Delta BL}$ ,  $\overline{\Delta V}$ , and  $\overline{\Delta a}$  to analyze the imperceptibility of the attack.  $\overline{\Delta BL}$  is the average absolute change per bone in the whole test set.  $\overline{\Delta V}$  and  $\overline{\Delta a}$  is the average absolute change per joint in the whole test. The lower these three metrics are, the sneakier the adversarial perturbations are. The results are shown in Table 10. To conveniently compare, we bold the worst errors in each time interval and the least change in each physical metric. In this experiment, we set  $\epsilon$  to 0.01 and attack the long-term models we train.

According to the result, our constraints weaken the attack effectiveness within an acceptable range meanwhile keep the adversarial example natural. Note that no constraints mean the original PGD method. Thus, the group with no physical constraints achieves the best attack effectiveness without considering any destructive influence on the human pose, which makes this group easy to be detected. On the contrary, our method with both constraints has the best imperceptibility and a little worse attack effectiveness, which meet the requirements of the attack to be adversarial and quasi-perceptible.

According to the comparison of the results from the two constraints, the temporal constraint and the bone-length constraint can complement each other in enhancing the naturalness of the example but not in weakening the attack’s effectiveness. Moreover, the temporal constraint is better in these two abilities than the bone-length constraint. The reason may be that the temporal constraint is versatile and can simultaneously attend to the bone length. In contrast, the bone-length constraint is a particular constraint to keep the skeleton with minor deformation that human agents can’t notice. Therefore, the two constraints limit the perturbation of a restricted space, which will not weaken the attack effectiveness too much.

## 7 Conclusion

This paper proposes the *first* adversarial attack against convolution-based human motion prediction and the first adversarial robustness evaluation of current convolution-based human motion predictors. The

experimental results show the models of human motion prediction are generally vulnerable to adversarial perturbation. As the analytical result, prior knowledge and semantic information can be critical to adversarial robustness. According to the quantitative and qualitative analysis, our adaptable scheme and two physical constraints effectively improve the attack generality across datasets and imperceptibility. In addition, the action prediction result from Multi-Head TrajectoryCNN indicates that the proposed attack barely influences the semantic information of the input sequence. Moreover, we shed light on the vulnerability of different frames in the input sequence, which shows the importance of caring more about the rear part of the input motion sequence.

## 8 Acknowledge

This work was supported partly by the National Natural Science Foundation of China (Grant No. 62173045, 62273054), partly by the Fundamental Research Funds for the Central Universities (Grant No. 2020XD-A04-3), and the Natural Science Foundation of Hainan Province (Grant No. 622RC675).

## References

- [1] Wei Mao, Miaomiao Liu, Mathieu Salzmann, and Hongdong Li. Learning trajectory dependencies for human motion prediction. In *Proceedings of the IEEE/CVF International Conference on Computer Vision*, pages 9489–9497, 2019.
- [2] Wei Mao, Miaomiao Liu, and Mathieu Salzmann. History repeats itself: Human motion prediction via motion attention. In *Computer Vision—ECCV 2020: 16th European Conference, Glasgow, UK, August 23–28, 2020, Proceedings, Part XIV 16*, pages 474–489. Springer, 2020.
- [3] Tiezheng Ma, Yongwei Nie, Chengjiang Long, Qing Zhang, and Guiqing Li. Progressively generating better initial guesses towards next stages for high-quality human motion prediction. In *Proceedings of the IEEE/CVF Conference on Computer Vision and Pattern Recognition*, pages 6437–6446, 2022.
- [4] Christian Szegedy, Wojciech Zaremba, Ilya Sutskever, Joan Bruna, Dumitru Erhan, Ian Goodfellow, and Rob Fergus. Intriguing properties of neural networks. *arXiv preprint arXiv:1312.6199*, 2013.
- [5] Seyed-Mohsen Moosavi-Dezfooli, Alhussein Fawzi, and Pascal Frossard. Deepfool: a simple and accurate method to fool deep neural networks. In *Proceedings of the IEEE Conference on Computer Vision and Pattern Recognition*, pages 2574–2582, 2016.
- [6] Aleksander Madry, Aleksandar Makelov, Ludwig Schmidt, Dimitris Tsipras, and Adrian Vladu. Towards deep learning models resistant to adversarial attacks. *arXiv preprint arXiv:1706.06083*, 2017.
- [7] Seyed-Mohsen Moosavi-Dezfooli, Alhussein Fawzi, Omar Fawzi, and Pascal Frossard. Universal adversarial perturbations. In *Proceedings of the IEEE Conference on Computer Vision and Pattern Recognition*, pages 1765–1773, 2017.
- [8] Nicholas Carlini and David Wagner. Towards evaluating the robustness of neural networks. In *2017 IEEE Symposium on Security and Privacy*, pages 39–57. IEEE, 2017.

- [9] Wieland Brendel, Jonas Rauber, and Matthias Bethge. Decision-based adversarial attacks: Reliable attacks against black-box machine learning models. *arXiv preprint arXiv:1712.04248*, 2017.
- [10] Jiawei Su, Danilo Vasconcellos Vargas, and Kouichi Sakurai. One pixel attack for fooling deep neural networks. *IEEE Transactions on Evolutionary Computation*, 23(5):828–841, 2019.
- [11] Cheng Luo, Qinliang Lin, Weicheng Xie, Bizhu Wu, Jinheng Xie, and Linlin Shen. Frequency-driven imperceptible adversarial attack on semantic similarity. In *Proceedings of the IEEE/CVF Conference on Computer Vision and Pattern Recognition*, pages 15315–15324, 2022.
- [12] Ziwen He, Wei Wang, Jing Dong, and Tieniu Tan. Transferable sparse adversarial attack. In *Proceedings of the IEEE/CVF Conference on Computer Vision and Pattern Recognition*, pages 14963–14972, 2022.
- [13] Ian J Goodfellow, Jonathon Shlens, and Christian Szegedy. Explaining and harnessing adversarial examples. *arXiv preprint arXiv:1412.6572*, 2014.
- [14] Zerui Chen, Yan Huang, and Liang Wang. On the robustness of 3d human pose estimation. In *2020 25th International Conference on Pattern Recognition (ICPR)*, pages 5326–5332. IEEE, 2021.
- [15] Moustapha Cisse, Yossi Adi, Natalia Neverova, and Joseph Keshet. Houdini: Fooling deep structured prediction models. *arXiv preprint arXiv:1707.05373*, 2017.
- [16] Qingzhao Zhang, Shengtuo Hu, Jiachen Sun, Qi Alfred Chen, and Z Morley Mao. On adversarial robustness of trajectory prediction for autonomous vehicles. In *Proceedings of the IEEE/CVF Conference on Computer Vision and Pattern Recognition*, pages 15159–15168, 2022.
- [17] Naman Jain, Sahil Shah, Abhishek Kumar, and Arjun Jain. On the robustness of human pose estimation. In *Proceedings of the IEEE/CVF Conference on Computer Vision and Pattern Recognition Workshops*, pages 29–38, 2019.
- [18] Jian Liu, Naveed Akhtar, and Ajmal Mian. Adversarial attack on skeleton-based human action recognition. *IEEE Transactions on Neural Networks and Learning Systems*, 33(4):1609–1622, 2020.
- [19] He Wang, Feixiang He, Zhexi Peng, Tianjia Shao, Yong-Liang Yang, Kun Zhou, and David Hogg. Understanding the robustness of skeleton-based action recognition under adversarial attack. In *Proceedings of the IEEE/CVF Conference on Computer Vision and Pattern Recognition*, pages 14656–14665, 2021.
- [20] Yunfeng Diao, Tianjia Shao, Yong-Liang Yang, Kun Zhou, and He Wang. Basar: black-box attack on skeletal action recognition. In *Proceedings of the IEEE/CVF Conference on Computer Vision and Pattern Recognition*, pages 7597–7607, 2021.
- [21] Tianhang Zheng, Sheng Liu, Changyou Chen, Junsong Yuan, Baochun Li, and Kui Ren. Towards understanding the adversarial vulnerability of skeleton-based action recognition. *arXiv preprint arXiv:2005.07151*, 2020.
- [22] Xiaoli Liu, Jianqin Yin, Jin Liu, Pengxiang Ding, Jun Liu, and Huaping Liu. Trajectorycnn: a new spatio-temporal feature learning network for human motion prediction. *IEEE Transactions on Circuits and Systems for Video Technology*, 31(6):2133–2146, 2020.

- [23] Xiaoli Liu and Jianqin Yin. Multi-head trajectorycnn: A new multi-task framework for action prediction. *Applied Sciences*, 12(11):5381, 2022.
- [24] Catalin Ionescu, Dragos Papava, Vlad Olaru, and Cristian Sminchisescu. Human3.6m: Large scale datasets and predictive methods for 3d human sensing in natural environments. *IEEE Transactions on Pattern Analysis and Machine Intelligence*, 36(7):1325–1339, 2013.
- [25] Timo Von Marcard, Roberto Henschel, Michael J Black, Bodo Rosenhahn, and Gerard Pons-Moll. Recovering accurate 3d human pose in the wild using imus and a moving camera. In *Proceedings of the European Conference on Computer Vision (ECCV)*, pages 601–617, 2018.
- [26] Lingwei Dang, Yongwei Nie, Chengjiang Long, Qing Zhang, and Guiqing Li. Msr-gen: Multi-scale residual graph convolution networks for human motion prediction. In *Proceedings of the IEEE/CVF International Conference on Computer Vision*, pages 11467–11476, 2021.
- [27] Judith Butepage, Michael J Black, Danica Kragic, and Hedvig Kjellstrom. Deep representation learning for human motion prediction and classification. In *Proceedings of the IEEE Conference on Computer Vision and Pattern Recognition*, pages 6158–6166, 2017.
- [28] Chen Li, Zhen Zhang, Wee Sun Lee, and Gim Hee Lee. Convolutional sequence to sequence model for human dynamics. In *Proceedings of the IEEE Conference on Computer Vision and Pattern Recognition*, pages 5226–5234, 2018.
- [29] Yanran Li, Zhao Wang, Xiaosong Yang, Meili Wang, Sebastian Iulian Poiana, Ehtzaz Chaudhry, and Jianjun Zhang. Efficient convolutional hierarchical autoencoder for human motion prediction. *The Visual Computer*, 35:1143–1156, 2019.
- [30] Maosen Li, Siheng Chen, Yangheng Zhao, Ya Zhang, Yanfeng Wang, and Qi Tian. Dynamic multiscale graph neural networks for 3d skeleton based human motion prediction. In *Proceedings of the IEEE/CVF Conference on Computer Vision and Pattern Recognition*, pages 214–223, 2020.
- [31] Qiongjie Cui, Huaijiang Sun, and Fei Yang. Learning dynamic relationships for 3d human motion prediction. In *Proceedings of the IEEE/CVF Conference on Computer Vision and Pattern Recognition*, pages 6519–6527, 2020.
- [32] Emre Aksan, Manuel Kaufmann, and Otmar Hilliges. Structured prediction helps 3d human motion modelling. In *Proceedings of the IEEE/CVF International Conference on Computer Vision*, pages 7144–7153, 2019.
- [33] Tim LeBailly, Sena Kiciroglu, Mathieu Salzmann, Pascal Fua, and Wei Wang. Motion prediction using temporal inception module. In *Proceedings of the Asian Conference on Computer Vision*, 2020.
- [34] Qiongjie Cui and Huaijiang Sun. Towards accurate 3d human motion prediction from incomplete observations. In *Proceedings of the IEEE/CVF Conference on Computer Vision and Pattern Recognition*, pages 4801–4810, 2021.
- [35] Bin Li, Jian Tian, Zhongfei Zhang, Hailin Feng, and Xi Li. Multitask non-autoregressive model for human motion prediction. *IEEE Transactions on Image Processing*, 30:2562–2574, 2020.
- [36] Chongyang Zhong, Lei Hu, Zihao Zhang, Yongjing Ye, and Shihong Xia. Spatio-temporal gating-adjacency gcn for human motion prediction. In *Proceedings of the IEEE/CVF Conference on Computer Vision and Pattern Recognition*, pages 6447–6456, 2022.



- [37] Theodoros Sofianos, Alessio Sampieri, Luca Franco, and Fabio Galasso. Space-time-separable graph convolutional network for pose forecasting. In *Proceedings of the IEEE/CVF International Conference on Computer Vision*, pages 11209–11218, 2021.
- [38] Xianjin Chao, Yanrui Bin, Wenqing Chu, Xuan Cao, Yanhao Ge, Chengjie Wang, Jilin Li, Feiyue Huang, and Howard Leung. Adversarial refinement network for human motion prediction. In *Proceedings of the Asian Conference on Computer Vision*, 2020.
- [39] Maosen Li, Siheng Chen, Yangheng Zhao, Ya Zhang, Yanfeng Wang, and Qi Tian. Multiscale spatio-temporal graph neural networks for 3d skeleton-based motion prediction. *IEEE Transactions on Image Processing*, 30:7760–7775, 2021.
- [40] Wei Mao, Miaomiao Liu, Mathieu Salzmann, and Hongdong Li. Multi-level motion attention for human motion prediction. *International Journal of Computer Vision*, 129(9):2513–2535, 2021.

## Appendix

### A Detailed prediction errors of the target models

Table A1: Short-term prediction errors of LTD on H3.6M before and after perturbation in variations of the boundary.

Intervals(ms)	80	160	320	400	80	160	320	400	80	160	320	400	80	160	320	400
scenarios	Walking				Eating				Smoking				Discussion			
LTD	8.9	15.7	29.2	33.4	8.8	18.9	39.4	47.2	7.8	14.9	25.3	28.8	9.8	22.1	39.6	44.1
$\epsilon=0.01$	35.5	71.0	123.2	137.0	29.6	61.4	114.9	130.6	27.0	56.5	104.8	119.0	32.9	70.6	123.2	130.8
$\epsilon=0.02$	49.1	97.5	171.1	189.4	41.4	83.0	152.4	173.6	36.1	74.5	140.0	159.2	42.8	87.6	144.9	150.5
$\epsilon=0.03$	54.8	109.2	202.5	225.2	49.6	98.1	<b>174.5</b>	<b>195.6</b>	45.4	94.2	<b>179.1</b>	<b>203.0</b>	51.7	105.5	186.1	201.0
$\epsilon=0.04$	62.5	122.5	212.9	230.7	52.3	98.2	168.7	188.2	48.5	97.0	173.3	192.7	57.8	117.1	201.9	215.6
$\epsilon=0.05$	<b>63.8</b>	<b>124.1</b>	<b>223.0</b>	<b>246.3</b>	<b>55.8</b>	<b>101.5</b>	164.2	178.1	<b>51.7</b>	<b>101.5</b>	178.6	196.8	<b>61.7</b>	<b>123.3</b>	<b>212.8</b>	<b>227.7</b>
scenarios	Direction				Greeting				Phoning				Posing			
LTD	12.6	24.5	48.1	58.3	14.5	30.5	74.2	89.0	11.5	20.3	37.9	43.2	9.5	24.0	66.2	83.0
$\epsilon=0.01$	35.6	71.5	126.2	142.5	36.9	80.1	163.2	183.7	32.4	64.9	118.1	132.9	38.5	86.5	185.8	218.3
$\epsilon=0.02$	48.2	96.1	166.1	183.1	46.1	99.2	194.5	216.3	39.1	74.1	129.2	145.3	51.0	108.7	216.5	247.8
$\epsilon=0.03$	51.6	100.1	167.2	183.7	52.8	112.6	216.3	239.2	48.6	92.9	162.5	179.1	57.3	118.5	228.7	258.5
$\epsilon=0.04$	52.0	97.3	158.2	173.1	54.8	113.1	210.9	230.9	51.4	<b>98.1</b>	<b>169.3</b>	<b>183.2</b>	60.5	118.7	221.6	250.1
$\epsilon=0.05$	<b>61.8</b>	<b>116.1</b>	<b>202.4</b>	<b>229.1</b>	<b>60.7</b>	<b>125.1</b>	<b>233.4</b>	<b>255.7</b>	<b>54.1</b>	<b>97.0</b>	<b>162.8</b>	<b>178.2</b>	<b>70.1</b>	<b>139.6</b>	<b>262.3</b>	<b>294.0</b>
scenarios	Purchase				Sitting				Sittingdown				Takingphoto			
LTD	19.6	38.6	64.5	72.2	10.7	24.5	50.6	62.0	11.4	27.6	56.4	67.6	6.8	15.2	38.2	49.6
$\epsilon=0.01$	41.8	83.5	137.3	146.2	36.7	82.5	158.7	180.1	35.7	78.9	154.9	175.7	26.7	58.2	118.9	137.6
$\epsilon=0.02$	51.8	99.6	164.1	174.6	45.8	97.8	179.7	200.9	46.9	99.7	189.4	212.8	37.5	77.5	147.1	165.2
$\epsilon=0.03$	56.1	106.0	172.1	182.6	60.0	<b>127.0</b>	<b>232.2</b>	<b>256.6</b>	52.7	104.3	189.3	211.9	49.9	<b>104.2</b>	<b>197.6</b>	<b>221.4</b>
$\epsilon=0.04$	62.8	118.7	196.3	<b>209.7</b>	59.8	121.6	215.7	237.3	54.1	106.2	188.3	207.9	<b>50.7</b>	100.6	182.2	201.7
$\epsilon=0.05$	<b>68.9</b>	<b>125.6</b>	<b>196.7</b>	206.1	<b>60.3</b>	122.7	217.5	238.4	<b>62.6</b>	<b>118.8</b>	<b>208.1</b>	<b>231.3</b>	47.1	88.6	159.8	177.9
scenarios	Waiting				Walkindog				Walkingtogether				Average			
LTD	9.5	22.0	57.5	73.9	32.2	58.0	102.3	122.8	8.9	18.4	35.3	44.3	12.2	25.0	51.0	61.3
$\epsilon=0.01$	37.7	80.1	152.5	169.6	55.6	101.8	174.0	195.2	29.3	61.2	105.1	119.5	35.5	73.9	137.4	154.6
$\epsilon=0.02$	48.4	99.4	181.7	201.9	64.2	119.6	204.4	225.5	39.8	80.7	142.0	162.0	45.9	93.0	168.2	187.2
$\epsilon=0.03$	56.4	113.2	201.2	219.6	71.6	132.6	224.1	245.6	48.2	96.4	165.7	187.0	53.8	107.6	193.3	214.0
$\epsilon=0.04$	<b>61.3</b>	<b>120.9</b>	<b>216.0</b>	<b>237.2</b>	74.8	137.6	<b>230.3</b>	<b>251.9</b>	<b>50.7</b>	<b>101.0</b>	<b>175.3</b>	<b>198.0</b>	56.9	111.2	194.7	213.9
$\epsilon=0.05$	60.4	115.4	201.0	218.3	<b>76.3</b>	<b>139.4</b>	230.2	250.0	49.0	97.2	164.7	181.1	<b>60.3</b>	<b>115.7</b>	<b>201.2</b>	<b>220.6</b>



Table A5: Short-term prediction errors of TrajectoryCNN on H3.6M before and after perturbation in variations of boundary.

Intervals(ms)	80	160	320	400	80	160	320	400	80	160	320	400	80	160	320	400
scenarios	Walking				Eating				Smoking				Discussion			
TrajCNN	8.3	15.2	31.3	36.3	8.6	18.9	38.0	45.6	6.3	12.8	23.7	28.0	7.8	20.3	41.7	48.0
$\epsilon=0.01$	37.7	85.4	164.3	177.1	38.8	87.9	175.7	194.5	29.2	64.8	130.7	148.2	42.3	97.7	189.7	205.4
$\epsilon=0.02$	60.5	134.1	259.1	279.9	55.1	120.9	231.2	249.4	43.8	95.4	186.9	211.2	62.2	139.0	259.2	275.5
$\epsilon=0.03$	71.8	155.2	298.3	319.5	64.3	136.7	252.9	270.8	51.2	110.1	214.6	240.1	70.3	150.4	273.9	293.4
$\epsilon=0.04$	75.6	160.6	299.6	318.0	68.4	142.3	259.5	277.1	53.5	112.8	218.1	<b>243.8</b>	76.9	165.0	<b>302.0</b>	<b>325.7</b>
$\epsilon=0.05$	<b>83.3</b>	<b>180.4</b>	<b>345.6</b>	<b>371.9</b>	<b>72.9</b>	<b>151.6</b>	<b>277.7</b>	<b>296.3</b>	<b>57.3</b>	<b>117.7</b>	<b>220.5</b>	242.9	<b>80.4</b>	<b>167.8</b>	299.6	319.1
scenarios	Direction				Greeting				Phoning				Posing			
TrajCNN	10.0	23.1	50.0	61.6	12.9	28.9	65.8	76.8	10.9	19.5	37.3	42.7	7.0	21.1	63.2	80.3
$\epsilon=0.01$	44.4	102.6	202.4	222.8	43.7	103.5	211.7	228.1	37.4	80.9	159.9	178.1	45.4	109.4	239.7	274.7
$\epsilon=0.02$	60.3	132.5	248.5	267.8	64.1	148.1	289.3	308.4	54.3	116.0	228.7	255.2	67.8	155.4	316.8	355.7
$\epsilon=0.03$	72.0	157.4	<b>297.9</b>	<b>324.8</b>	75.8	170.5	326.1	344.6	64.6	135.8	<b>259.6</b>	<b>284.9</b>	77.5	171.0	341.4	381.9
$\epsilon=0.04$	74.8	157.3	283.9	306.1	79.7	176.6	334.9	356.5	68.2	139.3	257.7	279.3	84.2	179.2	347.4	385.4
$\epsilon=0.05$	<b>78.6</b>	<b>162.1</b>	285.5	303.3	<b>84.4</b>	<b>184.5</b>	<b>349.9</b>	<b>374.1</b>	<b>68.7</b>	<b>139.7</b>	254.9	275.1	<b>87.3</b>	<b>185.9</b>	<b>360.5</b>	<b>401.1</b>
scenarios	Purchase				Sitting				Sittingdown				Takingphoto			
TrajCNN	17.4	37.6	68.2	78.7	9.3	23.0	48.3	60.3	11.9	30.9	61.3	69.4	5.4	13.6	38.8	50.8
$\epsilon=0.01$	47.3	108.0	214.6	240.8	37.1	89.7	187.4	214.2	40.7	99.1	198.2	220.6	39.5	92.1	195.3	224.4
$\epsilon=0.02$	64.2	142.7	271.7	299.2	55.3	128.9	256.9	285.8	58.3	134.7	260.4	286.4	56.4	126.9	255.8	287.5
$\epsilon=0.03$	72.7	156.6	289.0	317.2	65.3	147.2	287.0	317.4	67.3	150.2	287.7	315.7	68.0	149.9	290.8	322.0
$\epsilon=0.04$	78.4	168.2	<b>310.9</b>	<b>341.4</b>	66.2	145.7	281.5	309.4	70.0	148.5	275.7	299.4	73.1	<b>161.8</b>	<b>316.7</b>	<b>352.6</b>
$\epsilon=0.05$	<b>81.8</b>	<b>170.3</b>	305.6	329.8	<b>71.2</b>	<b>154.6</b>	<b>295.3</b>	<b>324.8</b>	<b>80.1</b>	<b>167.7</b>	<b>314.8</b>	<b>346.2</b>	<b>74.8</b>	161.2	307.5	338.6
scenarios	Waiting				Walkingdog				Walkingtogether				Average			
TrajCNN	8.0	20.3	53.5	70.1	22.2	50.2	99.7	116.8	8.2	18.3	34.5	43.0	10.3	23.6	50.3	60.6
$\epsilon=0.01$	41.7	95.8	190.0	208.2	44.5	102.9	199.0	221.8	34.6	79.0	149.4	161.5	40.3	93.3	187.2	208.0
$\epsilon=0.02$	63.3	139.2	260.6	280.0	60.4	137.6	262.0	287.0	55.6	126.2	247.7	270.5	58.8	131.8	255.7	280.0
$\epsilon=0.03$	72.4	156.2	292.4	316.5	69.5	151.7	266.9	284.7	65.7	146.3	276.6	298.7	68.6	149.7	283.7	308.8
$\epsilon=0.04$	77.6	165.1	308.8	<b>336.2</b>	76.6	167.5	302.6	323.0	71.1	155.1	290.2	311.9	72.9	156.3	292.6	317.7
$\epsilon=0.05$	<b>83.0</b>	<b>172.9</b>	<b>312.8</b>	332.6	<b>80.1</b>	<b>174.3</b>	<b>315.6</b>	<b>334.3</b>	<b>75.6</b>	<b>164.2</b>	<b>307.3</b>	<b>330.8</b>	<b>77.3</b>	<b>163.7</b>	<b>303.5</b>	<b>328.1</b>

Table A6: Long-term prediction errors of TrajectoryCNN on H3.6M before and after perturbation in variations of the boundary.

Intervals(ms)	560	1000	560	1000	560	1000	560	1000	560	1000	560	1000	560	1000	560	1000
scenarios	Walking		Eating		Smoking		Discussion		Direction		Greeting		Phoning		Posing	
TrajCNN	38.5	46.0	59.9	71.3	33.1	60.2	79.5	109.4	78.4	102.9	89.3	85.2	61.4	111.3	118.7	219.6
$\epsilon=0.01$	88.2	82.0	187.4	205.5	183.5	227.7	200.7	236.3	224.0	270.4	233.4	240.9	145.9	183.9	274.8	365.1
$\epsilon=0.02$	134.4	122.2	251.9	279.5	227.8	268.6	274.5	317.6	264.9	301.6	294.9	296.1	197.0	222.8	305.2	357.4
$\epsilon=0.03$	226.9	200.9	<b>277.0</b>	291.8	246.2	<b>284.1</b>	290.3	324.4	<b>313.7</b>	<b>350.8</b>	317.5	310.2	241.6	259.3	347.3	371.0
$\epsilon=0.04$	<b>264.7</b>	<b>253.7</b>	272.4	<b>299.1</b>	245.0	277.5	286.1	321.8	255.4	252.3	<b>335.6</b>	<b>333.4</b>	<b>246.2</b>	<b>262.6</b>	368.1	347.1
$\epsilon=0.05$	193.2	177.6	262.0	286.1	<b>249.3</b>	283.0	<b>320.1</b>	<b>360.3</b>	270.5	274.0	333.2	324.3	235.9	257.1	<b>389.4</b>	<b>394.7</b>
scenarios	Purchase		Sitting		Sittingdown		Takingphoto		Waiting		Walkingdog		Walkingtogether		Average	
TrajCNN	85.9	115.7	82.2	121.2	84.2	120.6	73.1	87.9	93.3	167.4	134.7	162.5	57.9	77.7	78.0	110.6
$\epsilon=0.01$	209.3	245.1	217.0	258.7	212.1	272.0	217.3	227.4	222.0	268.9	204.0	228.3	178.0	194.8	199.8	233.8
$\epsilon=0.02$	256.9	287.5	286.5	322.8	287.2	334.3	285.6	287.1	268.8	314.5	236.0	259.3	265.8	273.2	255.8	283.0
$\epsilon=0.03$	<b>320.4</b>	<b>353.4</b>	310.7	342.9	317.2	367.8	273.8	268.7	310.8	351.5	252.4	271.0	256.9	258.1	286.8	307.1
$\epsilon=0.04$	287.6	308.4	302.1	337.4	<b>355.3</b>	<b>407.8</b>	306.3	299.4	297.8	338.2	261.0	279.7	278.1	271.4	290.8	306.0
$\epsilon=0.05$	309.2	334.4	<b>312.0</b>	<b>347.6</b>	327.6	379.6	<b>329.1</b>	<b>329.4</b>	<b>325.5</b>	<b>364.8</b>	<b>265.7</b>	<b>295.6</b>	<b>315.0</b>	<b>300.3</b>	<b>295.8</b>	<b>313.9</b>

Table A7: Short-term prediction errors of TrajectoryCNN-50 on H3.6M before and after perturbation in variations of the boundary.

Intervals(ms)	80	160	320	400	80	160	320	400	80	160	320	400	80	160	320	400
scenarios	Walking				Eating				Smoking				Discussion			
TrajCNN-50	8.8	16.6	23.1	29.9	7.0	12.4	25.3	32.1	6.9	11.5	21.9	25.7	10.4	29.6	72.1	94.7
$\epsilon=0.01$	32.4	67.7	124.4	136.3	31.2	67.6	134.9	152.6	28.1	61.3	128.3	146.5	39.9	96.5	200.5	232.7
$\epsilon=0.02$	54.6	113.7	212.4	230.6	51.1	107.5	203.0	223.6	43.9	95.1	196.6	225.0	61.2	135.8	268.2	303.8
$\epsilon=0.03$	70.2	146.6	263.3	279.9	63.5	129.4	238.9	261.3	55.1	115.7	235.9	269.1	74.6	161.5	308.1	341.9
$\epsilon=0.04$	81.3	166.6	312.3	339.0	74.0	148.2	269.8	293.6	61.9	125.1	244.6	275.1	87.7	183.3	350.3	388.9
$\epsilon=0.05$	<b>96.2</b>	<b>195.9</b>	<b>351.4</b>	<b>372.2</b>	<b>82.5</b>	<b>160.7</b>	<b>278.7</b>	<b>296.4</b>	<b>74.0</b>	<b>150.8</b>	<b>298.2</b>	<b>336.6</b>	<b>98.8</b>	<b>201.3</b>	<b>373.5</b>	<b>410.9</b>
scenarios	Direction				Greeting				Phoning				Posing			
TrajCNN-50	5.8	15.6	41.9	60.0	13.3	29.2	59.3	80.6	8.9	21.0	40.1	49.7	9.7	27.7	69.2	88.8
$\epsilon=0.01$	41.3	95.3	189.6	214.7	35.8	78.2	150.4	176.4	34.7	77.5	152.2	172.9	38.1	100.8	231.9	271.5
$\epsilon=0.02$	61.3	132.3	251.1	279.0	55.4	118.6	227.8	258.0	54.5	116.9	217.6	242.6	59.2	147.4	320.5	366.7
$\epsilon=0.03$	75.2	158.7	293.1	320.8	71.4	148.3	265.9	288.5	69.9	145.5	268.0	297.5	74.8	176.2	364.8	412.3
$\epsilon=0.04$	87.1	179.7	328.1	357.3	84.5	172.1	297.4	312.5	81.1	167.3	308.3	342.3	88.3	202.6	405.8	452.0
$\epsilon=0.05$	<b>96.6</b>	<b>196.1</b>	<b>351.9</b>	<b>379.9</b>	<b>92.7</b>	<b>185.0</b>	<b>318.1</b>	<b>335.4</b>	<b>96.5</b>	<b>197.6</b>	<b>366.3</b>	<b>405.2</b>	<b>98.8</b>	<b>221.4</b>	<b>433.0</b>	<b>478.6</b>
scenarios	Purchase				Sitting				Sittingdown				Takingphoto			
TrajCNN-50	15.2	32.5	44.0	45.3	8.6	20.1	43.8	53.8	9.9	18.5	43.9	57.6	6.9	18.5	48.3	63.6
$\epsilon=0.01$	43.2	94.7	166.8	180.9	30.3	72.1	163.1	193.2	36.7	79.2	178.1	209.8	35.0	83.6	180.8	208.6
$\epsilon=0.02$	64.8	135.7	232.6	245.7	46.7	109.4	243.0	285.0	58.2	128.7	278.4	322.9	52.7	118.0	237.8	266.2
$\epsilon=0.03$	77.5	158.6	274.0	295.6	59.4	133.1	282.3	323.3	68.3	149.3	320.1	369.4	67.2	145.4	286.9	320.2
$\epsilon=0.04$	88.8	177.1	307.5	329.6	67.3	148.8	314.5	362.2	77.3	160.8	328.6	375.5	76.1	159.6	306.5	339.6
$\epsilon=0.05$	<b>105.5</b>	<b>205.9</b>	<b>351.7</b>	<b>374.0</b>	<b>76.5</b>	<b>167.4</b>	<b>353.6</b>	<b>407.7</b>	<b>88.5</b>	<b>184.3</b>	<b>378.1</b>	<b>431.3</b>	<b>85.9</b>	<b>174.9</b>	<b>325.7</b>	<b>356.2</b>
scenarios	Waiting				Walkingdog				Walkingtogether				Average			
TrajCNN-50	10.2	25.5	49.1	58.4	21.1	43.1	74.2	89.6	7.4	15.9	38.4	49.1	10.0	22.5	46.3	58.6
$\epsilon=0.01$	35.5	84.8	175.9	201.2	44.9	98.7	184.9	208.4	34.1	79.2	170.9	193.7	36.1	82.5	168.9	193.3
$\epsilon=0.02$	54.6	124.5	249.9	282.0	65.2	140.3	253.4	279.0	53.5	117.3	232.3	256.1	55.8	122.8	241.6	271.1
$\epsilon=0.03$	68.9	152.5	299.0	336.0	82.5	174.6	312.6	341.0	67.0	142.5	279.3	306.3	69.7	149.2	286.2	317.5
$\epsilon=0.04$	81.1	175.1	329.9	362.4	89.1	185.0	324.0	346.8	79.3	166.3	311.4	337.0	80.3	167.8	315.9	347.6
$\epsilon=0.05$	<b>93.1</b>	<b>195.0</b>	<b>360.5</b>	<b>393.7</b>	<b>104.5</b>	<b>212.3</b>	<b>367.8</b>	<b>396.0</b>	<b>89.6</b>	<b>184.5</b>	<b>342.4</b>	<b>369.5</b>	<b>92.0</b>	<b>188.9</b>	<b>350.1</b>	<b>382.9</b>

Table A8: Long-term prediction errors of TrajectoryCNN-50 on H3.6M before and after perturbation in variations of the boundary.

Intervals(ms)	560	1000	560	1000	560	1000	560	1000	560	1000	560	1000	560	1000	560	1000
scenarios	Walking		Eating		Smoking		Discussion		Direction		Greeting		Phoning		Posing	
TrajCNN-50	30.8	35.8	44.8	66.2	40.7	58.3	121.3	124.4	97.3	122.4	114.2	144.3	76.2	110.0	125.3	191.0
$\epsilon=0.01$	45.2	48.2	120.6	149.1	143.1	170.3	187.8	179.2	207.3	228.3	167.2	198.4	136.4	169.6	184.6	223.9
$\epsilon=0.02$	78.4	84.7	182.3	206.6	233.0	265.5	253.1	211.2	279.2	290.3	225.6	246.7	205.6	240.3	257.3	278.9
$\epsilon=0.03$	151.2	144.8	223.6	234.9	270.1	295.5	310.7	267.1	307.2	306.0	262.2	276.9	248.0	277.2	311.9	320.7
$\epsilon=0.04$	193.8	186.4	244.4	245.2	294.0	308.7	339.6	305.4	<b>383.0</b>	<b>397.8</b>	310.9	323.8	281.9	313.1	362.1	353.1
$\epsilon=0.05$	<b>272.9</b>	<b>262.2</b>	<b>310.7</b>	<b>330.2</b>	<b>318.3</b>	<b>339.5</b>	<b>386.4</b>	<b>362.4</b>	368.9	363.8	<b>345.9</b>	<b>365.0</b>	<b>317.0</b>	<b>340.2</b>	<b>399.6</b>	<b>380.1</b>
scenarios	Purchase		Sitting		Sittingdown		Takingphoto		Waiting		Walkingdog		Walkingtogether		Average	
TrajCNN	85.9	115.7	82.2	121.2	84.2	120.6	73.1	87.9	93.3	167.4	134.7	162.5	57.9	77.7	78.0	110.6
$\epsilon=0.01$	209.3	245.1	217.0	258.7	212.1	272.0	217.3	227.4	222.0	268.9	204.0	228.3	178.0	194.8	199.8	233.8
$\epsilon=0.02$	256.9	287.5	286.5	322.8	287.2	334.3	285.6	287.1	268.8	314.5	236.0	259.3	265.8	273.2	255.8	283.0
$\epsilon=0.03$	<b>320.4</b>	<b>353.4</b>	310.7	342.9	317.2	367.8	273.8	268.7	310.8	351.5	252.4	271.0	256.9	258.1	286.8	307.1
$\epsilon=0.04$	287.6	308.4	302.1	337.4	<b>355.3</b>	<b>407.8</b>	306.3	299.4	297.8	338.2	261.0	279.7	278.1	271.4	290.8	306.0
$\epsilon=0.05$	309.2	334.4	<b>312.0</b>	<b>347.6</b>	327.6	379.6	<b>329.1</b>	<b>329.4</b>	<b>325.5</b>	<b>364.8</b>	<b>265.7</b>	<b>295.6</b>	<b>315.0</b>	<b>300.3</b>	<b>295.8</b>	<b>313.9</b>

Table A9: Short-term prediction errors of HRI on H3.6M before and after perturbation in variations of the boundary.

Intervals(ms)	80	160	320	400	80	160	320	400	80	160	320	400	80	160	320	400
scenarios	Walking				Eating				Smoking				Discussion			
HRI	10.0	19.5	34.2	39.8	6.4	14.0	28.7	36.2	7.0	14.9	29.9	36.4	10.2	23.4	52.1	65.4
$\epsilon=0.01$	33.5	69.0	116.7	129.1	29.9	68.3	136.1	155.6	32.1	74.5	156.6	185.4	30.2	68.6	131.0	148.6
$\epsilon=0.02$	48.3	97.8	174.1	193.3	43.8	96.1	181.7	203.4	42.3	92.6	185.4	215.0	40.2	85.2	152.2	168.1
$\epsilon=0.03$	58.5	116.3	202.8	219.9	53.9	112.3	207.4	232.2	56.6	121.0	228.3	259.1	51.9	103.3	176.7	192.7
$\epsilon=0.04$	67.7	129.8	220.2	241.2	59.7	120.6	214.5	236.0	64.2	131.7	241.2	269.6	61.2	120.1	199.8	214.2
$\epsilon=0.05$	<b>71.5</b>	<b>135.7</b>	<b>232.2</b>	<b>256.7</b>	<b>67.9</b>	<b>131.5</b>	<b>230.9</b>	<b>254.7</b>	<b>76.0</b>	<b>152.1</b>	<b>265.4</b>	<b>291.4</b>	<b>67.4</b>	<b>128.3</b>	<b>215.9</b>	<b>235.5</b>
scenarios	Direction				Greeting				Phoning				Posing			
HRI	7.4	18.4	44.5	56.5	13.7	30.1	63.8	78.1	8.6	18.3	39.0	49.2	10.2	24.2	58.5	75.8
$\epsilon=0.01$	34.7	75.5	139.9	159.6	36.0	84.9	186.1	216.2	28.3	56.6	106.1	119.3	29.9	75.2	177.9	211.5
$\epsilon=0.02$	48.1	103.2	190.8	211.2	52.8	117.9	234.8	265.4	45.4	92.3	167.8	185.9	45.5	107.0	236.9	276.6
$\epsilon=0.03$	53.4	105.8	187.7	206.9	62.7	136.4	264.1	296.4	56.6	114.8	206.9	227.5	56.6	128.8	275.4	317.7
$\epsilon=0.04$	66.0	130.5	225.2	247.1	68.6	143.8	268.8	299.5	62.7	118.3	199.8	216.9	64.8	141.7	<b>296.0</b>	<b>341.6</b>
$\epsilon=0.05$	<b>68.0</b>	<b>132.3</b>	<b>231.2</b>	<b>253.1</b>	<b>73.2</b>	<b>151.4</b>	<b>284.3</b>	<b>319.0</b>	<b>65.7</b>	<b>124.6</b>	<b>211.6</b>	<b>229.6</b>	<b>68.0</b>	<b>144.8</b>	<b>289.9</b>	<b>329.3</b>
scenarios	Purchase				Sitting				Sittingdown				Takingphoto			
HRI	13.0	29.2	60.4	73.9	9.3	20.1	44.3	56.0	14.9	30.7	59.1	72.0	8.3	18.4	40.7	51.5
$\epsilon=0.01$	40.7	83.3	155.2	181.0	36.5	91.2	196.3	228.2	36.6	92.4	205.3	243.3	30.8	72.9	158.3	185.4
$\epsilon=0.02$	52.3	105.3	186.7	210.9	47.1	110.7	227.8	262.0	52.3	119.0	247.7	290.1	41.6	91.7	186.1	214.0
$\epsilon=0.03$	64.6	127.1	223.0	248.9	56.4	126.0	250.3	286.1	64.0	138.7	273.3	311.8	56.2	118.9	226.4	254.8
$\epsilon=0.04$	72.1	137.8	236.0	263.5	66.1	143.8	278.8	314.8	74.0	154.6	297.2	339.8	62.6	128.8	239.2	267.3
$\epsilon=0.05$	<b>77.6</b>	<b>147.1</b>	<b>249.1</b>	<b>273.5</b>	<b>74.4</b>	<b>158.1</b>	<b>297.6</b>	<b>332.0</b>	<b>83.0</b>	<b>167.2</b>	<b>307.4</b>	<b>344.4</b>	<b>72.1</b>	<b>146.3</b>	<b>269.1</b>	<b>298.5</b>
scenarios	Waiting				Walkingdog				Walkingtogether				Average			
HRI	8.7	19.2	43.4	54.9	20.1	40.3	73.3	86.3	8.9	18.4	35.1	41.9	10.4	22.6	47.1	58.3
$\epsilon=0.01$	44.4	95.2	184.0	208.3	52.4	102.5	188.3	214.3	42.4	91.2	172.4	198.4	46.6	100.5	194.4	221.1
$\epsilon=0.02$	63.3	139.2	260.6	280.0	60.4	137.6	262.0	287.0	55.6	126.2	247.7	270.5	58.8	131.8	255.7	280.0
$\epsilon=0.03$	56.0	114.9	209.0	234.2	61.1	117.5	211.3	237.5	53.7	113.5	211.2	237.8	57.5	119.7	223.6	250.9
$\epsilon=0.04$	61.9	126.5	<b>234.3</b>	<b>264.7</b>	70.9	137.6	247.1	277.3	62.9	130.1	236.9	262.0	65.7	133.0	242.3	270.4
$\epsilon=0.05$	<b>69.7</b>	<b>133.9</b>	227.7	251.1	<b>75.4</b>	<b>142.5</b>	<b>252.8</b>	<b>282.9</b>	<b>70.0</b>	<b>139.9</b>	<b>249.4</b>	<b>276.5</b>	<b>72.0</b>	<b>142.4</b>	<b>254.3</b>	<b>281.9</b>

Table A10: Long-term prediction errors of HRI on H3.6M before and after perturbation in variations of the boundary.

Intervals(ms)	560	1000	560	1000	560	1000	560	1000	560	1000	560	1000	560	1000
scenarios	Walking		Eating		Smoking		Discussion		Direction		Greeting		Phoning	
HRI	47.4	58.1	50.0	75.7	47.6	69.5	86.6	119.8	73.9	106.5	101.9	138.8	67.4	105.0
$\epsilon=0.01$	131.3	116.5	170.3	154.3	215.0	217.1	167.1	155.3	183.5	182.5	235.0	209.8	135.6	168.7
$\epsilon=0.02$	196.8	171.7	217.2	198.2	240.8	240.4	193.4	207.9	229.1	217.7	286.7	253.1	195.5	200.4
$\epsilon=0.03$	218.6	201.6	247.8	222.1	280.9	274.5	210.4	218.5	225.3	213.6	317.0	276.9	238.6	228.3
$\epsilon=0.04$	234.6	199.8	247.4	231.9	286.6	274.0	235.6	<b>248.7</b>	266.6	245.1	316.9	266.3	224.7	229.8
$\epsilon=0.05$	<b>262.9</b>	<b>224.4</b>	<b>261.7</b>	<b>238.0</b>	<b>302.9</b>	<b>284.6</b>	<b>250.2</b>	213.6	<b>271.2</b>	<b>251.8</b>	<b>342.7</b>	<b>298.8</b>	<b>244.5</b>	<b>244.4</b>
scenarios	Purchase		Sitting		Sittingdown		Takingphoto		Waiting		Walkingdog		Walkingtogether	
HRI	95.6	134.2	76.4	115.9	97.0	143.6	72.1	115.9	74.5	108.2	108.2	146.9	52.7	64.9
$\epsilon=0.01$	204.5	217.2	256.8	270.3	281.7	315.1	210.9	212.1	195.4	243.7	218.1	244.7	171.0	164.1
$\epsilon=0.02$	231.4	242.7	291.4	290.6	329.3	366.1	236.9	232.4	233.4	275.3	241.8	259.5	219.8	201.8
$\epsilon=0.03$	271.8	282.7	316.7	314.5	341.3	369.0	275.6	272.1	258.3	293.2	261.8	269.6	252.8	215.1
$\epsilon=0.04$	289.1	<b>289.8</b>	343.2	<b>341.6</b>	<b>372.6</b>	<b>407.8</b>	287.3	272.0	<b>296.4</b>	317.4	300.7	301.6	271.7	236.8
$\epsilon=0.05$	<b>290.2</b>	281.9	<b>351.5</b>	339.2	369.4	397.7	<b>319.0</b>	<b>293.9</b>	282.3	<b>331.1</b>	<b>309.5</b>	<b>312.3</b>	<b>292.2</b>	<b>263.4</b>
														<b>300.3</b>
														<b>288.4</b>



Table A14: Long-term prediction errors of LTD on CMU before and after perturbation in variations of the boundary.

Intervals(ms)	560	1000	560	1000	560	1000	560	1000	560	1000
scenarios	Basketball		Basketball signal		Directing traffic		Jumping		Running	
LTD	78.3	97.6	24.8	49.7	64.4	139.3	122.2	168.7	41.1	68.5
$\epsilon=0.01$	138.2	156.2	130.1	195.7	161.3	251.5	173.9	208.9	125.8	107.3
$\epsilon=0.02$	163.0	191.1	172.6	231.2	189.0	270.8	199.1	244.0	178.1	143.6
$\epsilon=0.03$	176.6	201.0	179.6	239.0	203.9	288.9	228.9	254.1	208.8	172.3
$\epsilon=0.04$	194.9	<b>228.5</b>	195.2	255.0	<b>218.2</b>	<b>299.4</b>	<b>231.9</b>	<b>267.2</b>	207.4	169.4
$\epsilon=0.05$	<b>200.1</b>	227.3	<b>206.7</b>	<b>263.8</b>	217.7	295.3	227.4	249.7	<b>223.1</b>	<b>185.8</b>
scenarios	Soccer		Walking		Wash window		Average			
LTD	87.1	119.8	28.8	34.5	55.3	81.7	62.7	95.0		
$\epsilon=0.01$	177.5	241.1	87.3	101.7	133.3	185.8	140.9	181.0		
$\epsilon=0.02$	202.5	260.2	119.4	131.5	159.9	216.4	173.0	211.1		
$\epsilon=0.03$	226.8	<b>297.3</b>	145.8	169.5	173.4	221.4	193.0	230.4		
$\epsilon=0.04$	<b>240.3</b>	292.8	172.1	<b>212.1</b>	169.5	211.5	203.7	242.0		
$\epsilon=0.05$	235.1	296.1	<b>180.4</b>	207.3	<b>181.3</b>	<b>240.9</b>	<b>209.0</b>	<b>245.8</b>		

Table A15: Short-term prediction errors of LTD-50 on CMU before and after perturbation in variations of the boundary.

Intervals(ms)	80	160	320	400	80	160	320	400	80	160	320	400
scenarios	Basketball				Basketball signal				Directing traffic			
LTD-50	11.0	20.4	43.7	57.0	2.6	4.8	10.3	13.4	6.4	12.2	27.8	37.4
$\epsilon=0.01$	23.2	42.3	84.5	101.5	14.5	27.8	57.1	64.7	18.7	37.4	81.1	97.0
$\epsilon=0.02$	26.8	49.7	100.6	118.9	21.6	42.4	91.2	104.4	24.4	49.1	105.7	124.2
$\epsilon=0.03$	29.9	54.7	107.2	126.4	26.8	51.7	111.8	128.6	27.7	53.8	112.6	131.6
$\epsilon=0.04$	33.9	61.2	118.7	138.6	32.1	61.2	<b>131.3</b>	<b>151.1</b>	31.1	60.2	126.8	146.6
$\epsilon=0.05$	<b>34.5</b>	<b>62.0</b>	<b>121.3</b>	<b>141.3</b>	<b>37.1</b>	<b>66.1</b>	128.5	144.8	<b>36.8</b>	<b>70.0</b>	<b>142.7</b>	<b>163.9</b>
scenarios	Jumping				Running				Soccer			
LTD-50	14.4	31.1	75.0	95.1	19.8	28.5	29.6	29.0	9.4	18.8	39.6	53.8
$\epsilon=0.01$	26.3	53.3	112.5	132.9	34.2	53.1	70.0	82.2	21.5	42.2	86.0	98.4
$\epsilon=0.02$	32.7	63.9	133.5	156.4	39.5	64.2	89.4	103.7	26.0	51.6	109.7	126.5
$\epsilon=0.03$	35.6	67.5	139.7	163.2	46.9	77.2	119.3	137.6	30.9	60.2	123.0	138.9
$\epsilon=0.04$	42.2	76.9	153.0	177.2	53.6	88.2	141.4	164.4	34.4	66.7	139.9	159.7
$\epsilon=0.05$	<b>46.3</b>	<b>82.2</b>	<b>160.0</b>	<b>184.3</b>	<b>57.2</b>	<b>92.7</b>	<b>144.8</b>	<b>165.5</b>	<b>38.3</b>	<b>73.7</b>	<b>150.4</b>	<b>171.1</b>
scenarios	Walking				Wash window				Average			
LTD-50	6.3	10.0	17.8	20.4	4.7	10.2	27.8	38.4	9.3	17.0	33.9	43.1
$\epsilon=0.01$	17.6	30.8	59.7	69.1	18.1	36.3	76.6	92.2	21.8	40.4	78.5	92.2
$\epsilon=0.02$	25.0	45.8	91.0	104.2	24.8	48.4	102.1	120.7	27.6	51.9	102.9	119.9
$\epsilon=0.03$	30.0	52.6	100.5	116.3	29.9	56.2	114.5	133.5	32.2	59.2	116.1	134.5
$\epsilon=0.04$	35.9	64.2	126.6	145.8	34.7	63.6	125.2	144.5	37.2	67.8	132.9	153.5
$\epsilon=0.05$	<b>41.5</b>	<b>71.8</b>	<b>135.1</b>	<b>154.2</b>	<b>38.2</b>	<b>69.9</b>	<b>142.5</b>	<b>165.5</b>	<b>41.2</b>	<b>73.6</b>	<b>140.7</b>	<b>161.3</b>

Table A16: Long-term prediction errors of LTD-50 on CMU before and after perturbation in variations of the boundary.

Intervals(ms)	560	1000	560	1000	560	1000	560	1000	560	1000
scenarios	Basketball		Basketball signal		Directing traffic		Jumping		Running	
LTD-50	77.2	102.4	24.7	53.0	69.1	134.9	126.6	159.8	42.6	77.2
$\epsilon=0.01$	116.8	141.5	112.2	170.0	138.7	227.8	152.1	180.0	85.9	78.6
$\epsilon=0.02$	139.1	168.6	153.3	198.5	165.4	248.6	165.3	199.9	110.5	84.3
$\epsilon=0.03$	154.5	183.6	170.2	207.7	179.0	262.9	175.5	209.1	131.0	100.5
$\epsilon=0.04$	171.5	198.7	205.6	<b>248.5</b>	196.1	281.2	192.4	<b>223.9</b>	145.5	109.8
$\epsilon=0.05$	<b>186.9</b>	<b>205.6</b>	<b>206.4</b>	240.6	<b>197.9</b>	<b>281.3</b>	<b>192.9</b>	217.3	<b>169.7</b>	<b>136.9</b>
scenarios	Soccer		Walking		Wash window		Average			
LTD-50	86.0	116.3	24.6	33.5	53.1	77.4	63.0	94.3		
$\epsilon=0.01$	136.9	187.7	59.5	66.5	107.8	166.7	113.7	152.4		
$\epsilon=0.02$	167.5	221.2	89.1	104.1	134.0	192.1	140.5	177.1		
$\epsilon=0.03$	212.1	275.5	116.7	126.7	139.9	199.6	159.9	195.7		
$\epsilon=0.04$	230.6	287.0	137.4	160.9	162.1	210.2	180.1	215.0		
$\epsilon=0.05$	<b>244.0</b>	<b>292.1</b>	<b>164.6</b>	<b>204.2</b>	<b>192.6</b>	<b>257.7</b>	<b>194.4</b>	<b>229.5</b>		



Table A17: Short-term prediction errors of TrajectoryCNN on CMU before and after perturbation in variations of the boundary.

Intervals(ms)	80	160	320	400	80	160	320	400	80	160	320	400
scenarios	Basketball				Basketball signal				Directing traffic			
TrajCNN	11.1	19.2	42.6	56.4	2.1	3.3	8.1	11.6	5.8	10.8	22.2	29.2
$\epsilon=0.01$	23.4	43.5	94.2	119.3	17.2	35.2	81.7	105.3	24.5	48.7	107.1	135.4
$\epsilon=0.02$	34.0	63.3	132.9	166.4	29.5	60.2	132.2	166.5	38.3	75.7	162.3	203.1
$\epsilon=0.03$	42.7	76.7	152.2	187.6	38.8	77.4	168.2	211.4	49.5	94.2	191.1	233.9
$\epsilon=0.04$	48.7	86.7	170.2	208.4	45.5	88.7	189.9	237.3	54.1	102.2	204.6	249.3
$\epsilon=0.05$	<b>54.9</b>	<b>95.9</b>	<b>183.4</b>	<b>221.7</b>	<b>52.2</b>	<b>99.2</b>	<b>209.1</b>	<b>260.8</b>	<b>62.9</b>	<b>115.3</b>	<b>222.3</b>	<b>265.8</b>
scenarios	Jumping				Running				Soccer			
TrajCNN	11.1	26.0	67.5	91.1	17.5	23.2	26.3	32.0	8.6	18.1	41.2	51.7
$\epsilon=0.01$	24.4	53.2	123.4	158.1	26.5	41.5	62.7	71.4	16.7	35.9	81.7	101.9
$\epsilon=0.02$	37.0	75.6	163.5	205.5	36.1	58.0	91.2	103.5	25.3	52.9	118.8	148.3
$\epsilon=0.03$	44.1	88.4	186.6	230.0	47.4	76.3	122.8	139.6	32.1	64.9	141.5	175.7
$\epsilon=0.04$	50.0	97.6	200.9	247.6	54.8	89.0	<b>145.1</b>	<b>165.8</b>	36.0	71.9	155.3	192.7
$\epsilon=0.05$	<b>57.5</b>	<b>109.2</b>	<b>222.5</b>	<b>271.3</b>	<b>58.5</b>	<b>89.4</b>	135.7	151.8	<b>40.9</b>	<b>79.0</b>	<b>165.6</b>	<b>204.0</b>
scenarios	Walking				Wash window				Average			
TrajCNN	6.7	10.7	19.5	24.1	4.7	10.3	31.6	44.1	8.4	15.2	32.4	42.5
$\epsilon=0.01$	19.3	38.4	83.1	104.3	24.3	50.7	120.2	153.9	22.0	43.4	94.3	118.7
$\epsilon=0.02$	30.0	59.4	129.5	161.5	37.5	74.4	160.6	199.9	33.5	65.0	136.4	169.3
$\epsilon=0.03$	38.2	72.9	152.2	187.8	50.1	95.5	204.6	255.0	42.9	80.8	164.9	202.6
$\epsilon=0.04$	42.6	79.2	162.1	198.8	57.1	108.4	223.8	273.6	48.6	90.4	181.5	221.7
$\epsilon=0.05$	<b>45.5</b>	<b>82.4</b>	<b>163.8</b>	<b>199.1</b>	<b>62.5</b>	<b>114.5</b>	<b>232.2</b>	<b>283.6</b>	<b>54.3</b>	<b>98.1</b>	<b>191.8</b>	<b>232.2</b>

Table A18: Long-term prediction errors of TrajectoryCNN on CMU before and after perturbation in variations of the boundary.

Intervals(ms)	560	1000	560	1000	560	1000	560	1000	560	1000
scenarios	Basketball		Basketball signal		Directing traffic		Jumping		Running	
TrajCNN	72.9	112.0	24.8	59.8	53.7	116.3	134.5	175.3	42.2	45.3
$\epsilon=0.01$	124.0	168.1	99.8	173.4	186.1	312.9	189.6	241.0	59.7	56.4
$\epsilon=0.02$	155.9	206.9	156.3	236.0	253.4	374.8	226.9	279.9	82.2	72.1
$\epsilon=0.03$	185.2	<b>241.1</b>	203.6	285.3	292.6	<b>412.0</b>	252.6	315.6	95.7	82.2
$\epsilon=0.04$	187.6	237.7	226.1	302.0	285.1	406.4	265.6	327.3	128.2	115.6
$\epsilon=0.05$	<b>191.5</b>	240.1	<b>226.7</b>	<b>316.2</b>	<b>302.9</b>	408.6	<b>289.9</b>	<b>350.6</b>	<b>158.3</b>	<b>147.6</b>
scenarios	Soccer		Walking		Wash window		Average			
TrajCNN	76.5	120.5	27.7	40.6	53.1	82.3	60.7	94.0		
$\epsilon=0.01$	125.2	192.2	94.3	129.1	151.0	209.3	128.7	185.3		
$\epsilon=0.02$	192.8	293.7	162.9	221.0	203.1	266.2	179.2	243.8		
$\epsilon=0.03$	211.6	312.4	183.0	249.7	236.4	296.0	207.6	274.3		
$\epsilon=0.04$	<b>243.6</b>	<b>333.8</b>	203.2	282.2	<b>255.4</b>	<b>323.7</b>	224.4	291.1		
$\epsilon=0.05$	227.0	317.7	<b>258.1</b>	<b>358.0</b>	254.9	318.0	<b>238.7</b>	<b>307.1</b>		

Table A19: Short-term prediction errors of TrajectoryCNN-50 on CMU before and after perturbation in variations of the boundary.

Intervals(ms)	80	160	320	400	80	160	320	400	80	160	320	400
scenarios	Basketball				Basketball signal				Directing traffic			
TrajCNN-50	11.8	19.7	41.4	53.6	1.8	3.1	7.4	10.6	5.8	11.7	25.6	34.1
$\epsilon=0.01$	19.4	34.6	70.7	88.4	15.8	31.5	70.1	90.0	17.1	36.4	82.4	105.4
$\epsilon=0.02$	27.8	50.4	101.9	125.8	30.0	60.1	130.6	164.2	28.5	59.1	131.9	167.2
$\epsilon=0.03$	36.3	65.5	127.2	154.9	39.5	75.8	160.1	200.6	36.6	73.8	155.9	192.7
$\epsilon=0.04$	45.3	80.4	153.9	185.7	49.1	93.3	185.7	224.5	47.3	91.9	188.1	230.8
$\epsilon=0.05$	<b>53.9</b>	<b>95.0</b>	<b>178.3</b>	<b>213.4</b>	<b>57.5</b>	<b>108.1</b>	<b>216.8</b>	<b>264.0</b>	<b>55.1</b>	<b>107.2</b>	<b>219.5</b>	<b>268.3</b>
scenarios	Jumping				Running				Soccer			
TrajCNN-50	11.5	26.3	68.2	92.0	19.3	29.5	29.7	33.2	8.5	19.9	48.1	60.0
$\epsilon=0.01$	23.0	47.7	106.2	135.1	30.0	48.7	61.8	66.6	16.5	36.0	83.5	103.0
$\epsilon=0.02$	36.6	71.8	147.5	182.5	41.8	68.8	94.7	101.0	26.5	56.0	124.2	152.0
$\epsilon=0.03$	49.7	93.5	184.3	224.5	52.6	86.3	120.8	127.5	34.1	69.3	150.0	183.1
$\epsilon=0.04$	60.9	110.4	209.1	248.8	60.8	97.4	136.0	142.8	42.8	86.1	185.2	226.3
$\epsilon=0.05$	<b>68.7</b>	<b>122.6</b>	<b>229.5</b>	<b>271.9</b>	<b>69.7</b>	<b>110.2</b>	<b>156.7</b>	<b>167.1</b>	<b>50.8</b>	<b>100.4</b>	<b>216.1</b>	<b>266.2</b>
scenarios	Walking				Wash window				Average			
TrajCNN-50	6.7	10.0	15.4	18.6	4.9	11.0	32.0	44.5	8.8	16.4	33.5	43.3
$\epsilon=0.01$	18.8	36.1	77.7	97.7	22.5	48.0	111.9	142.2	20.4	39.9	83.0	103.6
$\epsilon=0.02$	31.7	61.0	129.6	162.7	36.4	72.2	154.8	191.6	32.4	62.4	126.9	155.9
$\epsilon=0.03$	41.0	76.0	154.0	190.1	48.6	94.6	197.6	242.3	42.3	79.3	156.2	189.5
$\epsilon=0.04$	50.7	92.4	185.0	227.1	60.2	114.3	227.1	272.9	52.1	95.8	183.8	219.9
$\epsilon=0.05$	<b>57.1</b>	<b>103.1</b>	<b>205.9</b>	<b>252.7</b>	<b>65.5</b>	<b>121.1</b>	<b>238.9</b>	<b>288.2</b>	<b>59.8</b>	<b>108.5</b>	<b>207.7</b>	<b>249.0</b>

Table A20: Long-term prediction errors of TrajectoryCNN-50 on CMU before and after perturbation in variations of the boundary.

Intervals(ms)	560	1000	560	1000	560	1000	560	1000	560	1000
scenarios	Basketball		Basketball signal		Directing traffic		Jumping		Running	
TrajCNN-50	80.0	116.8	19.5	52.8	63.8	131.6	115.8	156.7	56.3	77.7
$\epsilon=0.01$	107.5	141.1	67.2	117.6	120.4	212.7	153.6	193.0	79.7	89.9
$\epsilon=0.02$	135.0	165.3	135.2	187.7	171.0	271.9	185.9	223.9	109.4	112.1
$\epsilon=0.03$	169.5	194.6	205.2	266.0	214.8	317.2	212.1	246.4	132.4	125.7
$\epsilon=0.04$	189.2	204.7	227.1	295.6	239.4	325.2	272.0	296.5	173.6	163.0
$\epsilon=0.05$	<b>211.4</b>	<b>230.1</b>	<b>271.1</b>	<b>342.4</b>	<b>261.7</b>	<b>359.1</b>	<b>293.0</b>	<b>314.4</b>	<b>173.7</b>	<b>159.1</b>
scenarios	Soccer		Walking		Wash window		Average			
TrajCNN-50	80.4	126.6	24.5	36.6	53.3	79.5	61.7	97.3		
$\epsilon=0.01$	125.7	191.0	53.1	58.2	115.8	154.4	102.9	144.7		
$\epsilon=0.02$	184.3	254.9	145.3	188.8	171.2	221.2	154.7	203.2		
$\epsilon=0.03$	219.2	279.3	212.2	268.7	224.6	287.9	198.7	248.2		
$\epsilon=0.04$	243.6	294.9	261.8	326.3	<b>256.9</b>	<b>316.0</b>	232.9	277.8		
$\epsilon=0.05$	<b>255.7</b>	<b>302.3</b>	<b>280.4</b>	<b>344.4</b>	245.8	298.4	<b>249.1</b>	<b>293.8</b>		

Table A21: Short-term prediction errors of HRI on CMU before and after perturbation in variations of the boundary.

Intervals(ms)	80	160	320	400	80	160	320	400	80	160	320	400
scenarios	Basketball				Basketball signal				Directing traffic			
HRI	12.4	22.8	50.5	65.6	2.7	4.6	9.8	13.1	5.8	11.9	26.5	35.6
$\epsilon=0.01$	20.6	43.9	109.3	144.2	21.6	50.1	127.1	167.6	20.4	47.7	114.5	148.6
$\epsilon=0.02$	28.6	59.8	144.9	189.6	34.2	73.2	170.2	217.6	31.1	68.7	160.5	206.3
$\epsilon=0.03$	36.1	73.1	171.1	221.1	39.5	80.5	180.4	228.9	39.4	81.6	182.2	232.6
$\epsilon=0.04$	44.2	86.3	192.6	245.7	45.6	89.1	192.1	240.6	42.7	87.2	193.6	246.0
$\epsilon=0.05$	<b>50.1</b>	<b>96.5</b>	<b>209.9</b>	<b>265.6</b>	<b>51.4</b>	<b>98.8</b>	<b>209.9</b>	<b>261.7</b>	<b>50.6</b>	<b>101.3</b>	<b>217.9</b>	<b>273.1</b>
scenarios	Jumping				Running				Soccer			
HRI	13.6	27.9	66.3	86.0	19.7	27.3	28.8	30.3	10.2	20.0	42.6	54.3
$\epsilon=0.01$	25.0	52.9	126.8	164.9	32.4	55.6	109.1	137.4	19.3	43.9	108.3	142.2
$\epsilon=0.02$	35.2	73.4	169.2	217.2	47.0	84.5	157.0	193.2	29.7	65.7	156.5	203.3
$\epsilon=0.03$	45.0	89.3	198.5	250.9	58.8	104.6	192.1	232.4	35.4	76.1	176.5	227.7
$\epsilon=0.04$	51.2	96.8	207.1	259.8	67.3	118.3	215.9	260.3	41.2	85.1	188.8	240.3
$\epsilon=0.05$	<b>60.5</b>	<b>113.6</b>	<b>239.0</b>	<b>297.8</b>	<b>73.6</b>	<b>127.4</b>	<b>233.7</b>	<b>281.8</b>	<b>45.5</b>	<b>91.7</b>	<b>200.5</b>	<b>256.1</b>
scenarios	Walking				Wash window				Average			
HRI	6.4	10.4	17.9	21.8	5.2	11.0	29.1	39.0	9.5	17.0	33.9	43.2
$\epsilon=0.01$	19.2	41.9	101.5	130.6	22.0	49.2	119.8	155.2	22.6	48.1	114.5	148.8
$\epsilon=0.02$	32.6	66.9	151.0	191.6	34.6	72.3	162.5	204.7	34.1	70.6	159.0	202.9
$\epsilon=0.03$	42.1	83.4	182.1	228.4	40.7	80.5	173.7	218.0	42.1	83.6	182.1	230.0
$\epsilon=0.04$	48.1	90.8	189.2	235.2	48.6	92.5	192.4	238.2	48.6	93.3	196.5	245.8
$\epsilon=0.05$	<b>54.7</b>	<b>101.7</b>	<b>211.1</b>	<b>260.4</b>	<b>55.6</b>	<b>101.6</b>	<b>204.9</b>	<b>251.9</b>	<b>55.3</b>	<b>104.1</b>	<b>215.9</b>	<b>268.6</b>

Table A22: Long-term prediction errors of HRI on CMU before and after perturbation in variations of the boundary.

Intervals(ms)	560	1000	560	1000	560	1000	560	1000	560	1000
scenarios	Basketball		Basketball signal		Directing traffic		Jumping		Running	
HRI	90.1	126.3	21.2	48.2	59.9	136.8	116.4	175.4	35.0	70.7
$\epsilon=0.01$	206.0	268.1	239.6	320.7	220.1	323.0	231.2	334.3	186.5	230.0
$\epsilon=0.02$	266.2	337.4	290.1	348.9	289.0	377.7	288.8	369.0	250.3	269.9
$\epsilon=0.03$	303.3	376.5	303.2	362.6	314.8	403.8	329.3	416.8	292.3	305.3
$\epsilon=0.04$	328.4	393.2	309.8	368.4	331.2	412.2	329.3	401.3	325.3	349.4
$\epsilon=0.05$	<b>349.4</b>	<b>421.9</b>	<b>334.7</b>	<b>387.5</b>	<b>357.3</b>	<b>431.4</b>	<b>375.9</b>	<b>430.3</b>	<b>350.8</b>	<b>372.7</b>
scenarios	Soccer		Walking		Wash window		Average			
HRI	76.6	130.1	26.8	33.9	52.5	91.3	59.8	101.6		
$\epsilon=0.01$	203.8	277.1	188.1	244.6	211.1	288.2	210.8	285.8		
$\epsilon=0.02$	283.0	339.4	258.6	313.7	264.8	328.4	273.8	335.5		
$\epsilon=0.03$	313.7	378.5	302.8	359.2	280.3	336.0	305.0	367.4		
$\epsilon=0.04$	324.0	383.3	304.0	353.5	299.9	<b>358.0</b>	319.0	377.4		
$\epsilon=0.05$	<b>340.7</b>	<b>396.2</b>	<b>335.2</b>	<b>385.2</b>	<b>311.0</b>	354.3	<b>344.4</b>	<b>397.4</b>		

Table A23: Short-term prediction errors of Multi-head TrajectoryCNN on CMU before and after perturbation in variations of the boundary.

Intervals(ms)	80	160	320	400	80	160	320	400	80	160	320	400
scenarios	Basketball				Basketball signal				Directing traffic			
MH-TrajCNN	11.6	20.6	43.0	56.5	2.4	5.0	11.9	15.9	6.2	12.8	29.1	39.8
$\epsilon=0.01$	16.6	28.7	57.5	73.2	9.8	15.6	28.0	34.0	12.3	22.4	46.3	59.9
$\epsilon=0.02$	23.6	38.7	74.3	92.6	18.8	29.5	52.2	62.3	20.2	35.1	68.2	85.5
$\epsilon=0.03$	30.4	49.4	91.4	111.8	28.7	45.2	82.1	99.4	29.5	50.7	96.8	119.3
$\epsilon=0.04$	38.3	61.9	110.1	132.6	39.4	61.3	108.0	129.7	37.1	62.6	118.6	144.2
$\epsilon=0.05$	<b>45.4</b>	<b>70.7</b>	<b>122.9</b>	<b>146.4</b>	<b>45.9</b>	<b>69.9</b>	<b>118.9</b>	<b>140.0</b>	<b>45.0</b>	<b>76.6</b>	<b>146.5</b>	<b>178.9</b>
scenarios	Jumping				Running				Soccer			
MH-TrajCNN	14.1	29.7	72.0	94.1	21.9	29.9	38.0	44.4	8.6	19.7	48.3	62.2
$\epsilon=0.01$	22.5	42.4	91.8	115.3	28.6	42.3	63.2	72.9	14.0	28.3	62.6	77.9
$\epsilon=0.02$	33.5	57.9	114.4	139.7	39.7	59.6	89.9	102.3	21.6	41.5	87.5	108.0
$\epsilon=0.03$	44.4	73.8	139.5	168.2	50.1	75.4	111.4	124.4	30.6	57.0	119.2	148.0
$\epsilon=0.04$	56.8	93.6	173.0	207.0	62.8	93.4	136.0	150.5	37.5	66.9	134.4	164.2
$\epsilon=0.05$	<b>66.5</b>	<b>107.3</b>	<b>194.3</b>	<b>231.5</b>	<b>73.0</b>	<b>105.9</b>	<b>148.4</b>	<b>162.4</b>	<b>45.0</b>	<b>79.5</b>	<b>158.2</b>	<b>194.0</b>
scenarios	Walking				Wash window				Average			
MH-TrajCNN	7.5	10.9	16.8	19.2	5.6	12.8	36.2	48.3	9.7	17.7	36.9	47.5
$\epsilon=0.01$	15.2	23.2	36.3	41.0	15.3	29.0	63.6	79.9	16.8	29.0	56.2	69.3
$\epsilon=0.02$	25.2	39.8	68.0	79.9	26.0	45.8	90.8	111.2	26.1	43.5	80.7	97.7
$\epsilon=0.03$	35.7	56.9	99.7	118.4	39.0	67.8	131.3	159.3	36.0	59.6	108.9	131.1
$\epsilon=0.04$	46.2	75.2	139.2	168.4	48.4	80.5	148.7	178.4	45.8	74.4	133.5	159.4
$\epsilon=0.05$	<b>53.5</b>	<b>84.7</b>	<b>146.7</b>	<b>172.8</b>	<b>61.0</b>	<b>99.2</b>	<b>177.1</b>	<b>209.3</b>	<b>54.4</b>	<b>86.7</b>	<b>151.6</b>	<b>179.4</b>

Table A24: Long-term prediction errors of Multi-head TrajectoryCNN on CMU before and after perturbation in variations of the boundary.

Intervals(ms)	560	1000	560	1000	560	1000	560	1000	560	1000
scenarios	Basketball		Basketball signal		Directing traffic		Jumping		Running	
MH-TrajCNN	84.1	126.5	32.7	73.3	71.7	135.4	118.7	158.8	65.0	76.1
$\epsilon=0.01$	97.2	137.2	56.0	102.1	102.1	177.9	142.0	180.1	86.6	88.9
$\epsilon=0.02$	116.5	154.7	97.4	156.6	133.7	219.5	166.6	201.1	106.7	100.8
$\epsilon=0.03$	133.8	171.5	116.7	177.1	167.0	264.5	202.8	239.4	131.0	120.2
$\epsilon=0.04$	147.2	182.1	148.6	215.2	192.3	290.4	233.4	270.4	160.1	147.1
$\epsilon=0.05$	<b>166.4</b>	<b>199.2</b>	<b>169.5</b>	<b>237.6</b>	<b>204.8</b>	<b>297.6</b>	<b>269.0</b>	<b>301.1</b>	<b>204.0</b>	<b>194.7</b>
scenarios	Soccer		Walking		Wash window		Average			
MH-TrajCNN	86.6	128.3	26.2	41.1	61.8	86.7	68.4	103.3		
$\epsilon=0.01$	124.7	174.9	54.0	71.3	87.6	110.1	93.8	130.3		
$\epsilon=0.02$	170.8	237.2	101.4	131.5	122.6	151.4	127.0	169.1		
$\epsilon=0.03$	202.0	276.6	201.2	270.7	160.7	197.6	164.4	214.7		
$\epsilon=0.04$	240.5	309.7	239.3	307.8	198.0	236.3	194.9	244.9		
$\epsilon=0.05$	<b>265.4</b>	<b>335.4</b>	<b>261.9</b>	<b>325.2</b>	<b>224.5</b>	<b>261.7</b>	<b>220.7</b>	<b>269.1</b>		

## B Discussion about the Non-Monotonic Growth

According to the results in the Tabel A1-A24, the non-monotonic growth of specific activities' MPJPE as  $\epsilon$  or time interval grows happens differently among models. Based on our observation, LTD encounters this non-monotonic growth phenomenon as  $\epsilon$  is enlarged more than TrajectoryCNN, with HRI following behind. In contrast, Multi-Head TrajectoryCNN hardly meets such a phenomenon. Note that our adversarial attack only affects the output by perturbing input data while the algorithm still models the predicted motion. Although the disturbed output is far from the ground truth, its output still follows the motion that the algorithm comprehends, which cannot determine the concrete location of the joints in our attack method. The increment of  $\epsilon$  indicates the increment of the attack intensity. If the  $\epsilon$  alteration can change the errors directly, the model thoroughly understands the perturbed human motion sequence. Therefore, the ranking above can be considered as the ranking of how thoroughly the models comprehend the relation between the history and future motion sequence. The classification head of the Multi-Head TrajectoryCNN directly helps its comprehension of human motion, which is why it hardly meets the phenomenon. The attention mechanism helps HRI focus on the critical feature of human motion, which boosts the understanding of human motion in HRI. TrajectoryCNN and LTD do not have direct enhancements, so they fall back in the ranking. Comparing the results between LTD and LTD-50, or TrajCNN and TrajCNN-50, we can find that the non-monotonic phenomenon happens much less, which indicates that increasing the input length is a simple way to support the model.

Contrary to the above ranking, the ranking of meeting the non-monotonic growth of errors as the

time interval is enlarged from frequent to occasional is HRI, Multi-Head TrajectoryCNN, LTD, TrajectoryCNN. Except for the sudden decrease caused by changing model, the non-monotonic growth along time intervals only happens in long-term prediction. Except for the results of HRI, Most activities meet this phenomenon after  $\epsilon$  reaches 0.03. Only “greeting” predicted by LTD, the results of TrajectoryCNN on 3DPW, the results of HRI on Human 3.6M and 3DPW, “discussion,” “waiting,” “walking together,” and “running” predicted by Multi-Head TrajectoryCNN are earlier than others. Clean “greeting” motion prediction of LTD also has non-monotonic growth. Therefore, finding the same trend under attack is possible. The predicted sequence begins from the last pose the model observed, so short-term predictions are within a limited range and will not face non-monotonic growth. As the time interval enlarged, the possibility of predicted joints’ location increased. Therefore, non-monotonic growth is observed in a wide range. To figure out what kind of activity will cause the non-monotonic growth, we find “walking,” “waiting,” “eating,” “greeting,” “walking together,” and “running” encounter the phenomenon. Empirically, these activities are regular or rapid. The activities from 3DPW are varied from the other two datasets, which contain more activities under wild conditions. As a result, distances between the perturbed prediction and ground truth of these activities are hard to be determined even though we maximize the average error. However, half of the activities predicted by HRI meet the non-monotonic growth along time intervals. This may be because HRI utilizes the predicted sequence as the input to reach the long-term prediction, and finally, the prediction will be more and more out of control.